COMPUTER SIMULATIONS OF SELF-ASSEMBLED MONOLAYERS ON THE AU (111) SURFACE

By

SABRI ALKIS

A DISSERTATION PRESENTED TO THE GRADUATE SCHOOL
OF THE UNIVERSITY OF FLORIDA IN PARTIAL FULFILLMENT
OF THE REQUIREMENTS FOR THE DEGREE OF
DOCTOR OF PHILOSOPHY

UNIVERSITY OF FLORIDA

2009

To my family

ACKNOWLEDGEMENTS

I thank my parents and my research committee members, Nicolo Omenetto, Adrian Roitberg, Hai-Ping Cheng and So Hirata for support. I also would like to acknowledge my research group members Julio Palma, Christina Crecca, Luis Agapito, Josh McClellan. Their help is greatly appreciated in this work. I also thank Department of Energy (DOE) for supporting our research.

TABLE OF CONTENTS

page

LIST OF TABLES

LIST OF FIGURES

Abstract of Dissertation Presented to the Graduate School
of the University of Florida in Partial Fulfillment of the
Requirements for the Degree of Doctor of Philosophy

COMPUTER SIMULATIONS OF SELF-ASSEMBLED MONOLAYERS ON THE AU (111) SURFACE

By

Sabri Alkis

May 2009

Chair: Jeffrey Krause
Major: Chemistry

Many polymer and organic molecule assemblies have been investigated recently because of their applications in molecular electronics, surface chemistry and bio-sensors. These assemblies are often used in surface studies because they are simple structurally, stable thermodynamically and have well-defined order. Great effort has been made to understand the properties of these systems both experimentally and theoretically. Computer simulations in collaboration with experiments help us understand these systems in greater detail.

In the first project, heterogeneous systems containing of a host alkanethiol molecule (dodecanethiol) monolayer with a thiol-terminated azobenzene molecules were considered. Classical molecular dynamics simulations showed a phase transition that was characterized by the change in the tilt angle, heat capacity and diffusion constant of the host molecules. The results for the pure monolayer were compared to the heterogeneous systems and the results were used to describe recent experiments. The phase transition was found to occur at about 350K for all three systems which is in good agreement with the experimental results.

In the second project, motions of Au atoms on alkanethiol monolayers were described using classical molecular dynamics in conjunction with first principle calculations. Based on quantum-mechanical calculations, the interaction between Au atoms and the monolayer was

calibrated and then the motions of the atoms were investigated as a function of coverage and temperature. We found good agreement with experimental results. Gold atoms were observed to penetrate inside the monolayer at room temperature but not below room temperature.

In the third project, inspired by recent experiments, we used classical molecular dynamics to study the motions of Ag_n clusters with various sizes on alkanethiol self-assembled monolayers. Detailed results on the dynamics, diffusion and sintering processes of these nano-clusters were reported.

CHAPTER 1
INTRODUCTION

Prologue

Self-assembled monolayers (SAMs) offer researchers great opportunities to understand self-organization and structure-property relationship,[1] as they are highly ordered and oriented. Therefore, it is possible to produce a variety of surfaces with specific interactions. It is possible to change both the tails and the head groups of the molecules, which provides the opportunity to understand intermolecular, molecule-substrate and molecule-solvent interactions.[2] These systems are well-defined and they are easily accessible, which makes them good model systems to study chemistry and physics in two dimensions.[2]

Since they have a dense and a fairly stable structure, SAMs have potential applications in corrosion prevention and wear protection.[3] They also have a biocompatible nature, which makes them applicable in chemical and bio-chemical sensing. They are highly ordered and are ideal components in electro-optic devices.[4]

In this chapter general information about self-assembled monolayers, their preparation and their chemical applications is presented. Pioneering theoretical work to study these monolayers is also described. Finally, an overview of the research projects in the thesis is presented.

Self Assembled Monolayers, Structure and Formation

Self-assembly can be described as the formation of complex structures from small building blocks. In nature, self-assembly is observed in the formation of membranes from lipid molecules. Living cells are also good examples of self-assembly. Adsorption of a surfactant with a specific affinity to a substrate leads to the formation of self-assembled monolayers.[5] Chemical bond formation of molecules with surface and intermolecular interactions acts as a driving force for the formation of self-assembled monolayers.[5]

These types of assemblies are important because they can be prepared easily. Their surface properties can be changed easily through the modification of molecular structure and functions. It is also possible to use self-assembled monolayers as building blocks in more complex structures. They can be used, for example, to dock additional layers to a surface.[5]

Over the last 15 years, the field of self-assembled monolayers has been a very popular research topic and many self-assembled monolayers have been investigated. The monolayers of organosulfur adsorbates (e.g., alkanethiols) on gold are probably the most well-studied.[2]

Sulfur compounds are known to have a strong affinity to transition metal surfaces such as the gold surface.[6, 7] The reason is the possibility of forming multiple bonds with the surface metal.[8] A variety of organosulfur derivatives have now been studied. Some of these derivatives are di-n-alky-sulfate,[9, 10] thiophenols,[11, 12] mercaptopyridines[12] and mercaptoanilines.[13] Among these derivatives, alkanethiols on Au(111) are the most well-studied and best understood.[12]

Adsorption of alkanethiols on a Au(111) surface occurs in two steps: A very fast step that takes only a few minutes and a slow step which takes several hours. At the end of the first step, the thickness reaches the 80-90 % of its maximum value. After the second step the thickness and the contact angles reach their final values.[14] This two step mechanism is confirmed by X- ray photoelectron spectroscopy (XPS) measurements,[15, 16] and near edge X-ray absorption fine structure (NEXAFS) studies.[17]

Results from the electron diffraction studies show that the monolayers of alkanethiols on a Au(111) surface have hexagonal symmetry with an S-S spacing of 4.97 Å. The calculated area per molecule is 21.4 $Å^2$. The structure is a simple $\sqrt{3}x\sqrt{3}R\ 30^0$ lattice which is confirmed by helium diffraction[18] and atomic force microscopy (AFM)[19] studies.

Alkanethiolates on a Au(111) surface are tilted 26-28^0 from the surface normal at around 50 K and have 52-55^0 rotation about the molecular axis. The alkanethiols tilt to reestablish van der Waals contact in an assembly with S-S distances of about 5 Å. This distance is larger than the distance of 4.6 Å that is reported for perpendicular alkyl chains.[2]

Applications

SAMs have several technical applications such as surface coatings, molecular electronics and active elements in sensors.[5] One application of SAMs is corrosion protection.[20-24] They can also be employed in mechanical protection of surfaces. SAMs have been used to modify iron and steel surfaces to make them more resistant.[25, 26] It is also possible to change the end-groups (hydrophobic, hydrophilic) to control the wetting properties. Changing the end-groups also helps to change the mechanical properties relevant to friction and lubrication.[27, 28]

SAMs can also be used as building blocks in heterostructures, as templates to initiate the growth of the adlayer. Further layers might be attached to the material using these SAMs.[5] They have also been used to start polymerization by chemically anchoring the adlayer. An example might be ZrO_2 in nanocrystalline ceramics.[29, 30]

They could form a link between organic and inorganic matter which makes them ideal for interfacing biological materials. The could be used for filtering and analytical purposes in bio-technology.[31] SAMs of alkanethiol molecules on a Au(111) surface that present tri-(propylene sulfoxide) groups prevent the non-specific adsorption of protein that is confirmed by surface plasmon resonance (SPR) spectroscopy.[31]

Another example would be the transducer technology, various forms of chemical, optical, piezoelectric sensors have been made using SAMs.[32] X-ray photoelectron spectroscopy (XPS) results show that, it is possible to detect small organic molecules such as C_2Cl_4 by alkanethiol

molecules on a Au(111) surface.[32] Tailoring the chain groups leads to detection of gaseous analytes.[33, 34]

These systems also serve as test beds for investigations of properties of possible new-generation molecular-electronic devices. The alkanethiol SAM presents a classical metal-insulator-metal (MIM) tunnel junction when fabricated between metal contacts due to their large HOMO-LUMO gap (HOMO: highest occupied molecular orbital; LUMO: lowest unoccupied molecular orbital) of approximately 8 eV.[35-37]

From Experiment to Theory

To simulate the SAMs, various models and approximations have been used. Researchers have focused on various aspects such as the headgroup bonding structure or the thermal behavior of the chains.[5]

Pioneering simulations of SAMs were preformed by the Klein group.[38, 39] They used a structureless model potential with united-atom approximation. Since then, various force fields have been used to describe the behavior of these monolayers. Most of the simulations have yielded the $(\sqrt{3}x\sqrt{3})\ R30^0$ structure with a tilt angle of about 28 degrees.[2] These simulations also reported the thermal behavior and the disordering (melting) transition.[39-41]

Bhatia and Garrison[42] did molecular dynamics studies in which the sulfur groups were left mobile on the Au(111) surface. Again, they used the united-atom model to describe the molecular potentials. They observed the change in tilt angles and the phase transition in the monolayers. Beardmore[43] developed an empirical potential function by fitting parameters of the Au-S interaction to quantum calculations.

Overview of Research Projects

Classical molecular dynamic simulations were used with quantum-mechanical calculations to simulate the behavior of these systems and their applications in molecular electronics.

First Project: Simulations of Azobenzene Containing Alkanethiol SAMs on the Au(111) Surface

In our first project, we simulated alkanethiol monolayers with an azobenzene molecule on the Au(111) surface. We characterized a phase transition by looking at the change in tilt angles, heat capacity and the diffusion constant of the host molecules. We observed a phase transition at about 350 K which agrees well with the experimental results. The results of these simulations were published in Journal of Physical Chemistry C.[45]

Second Project: Molecular Dynamics Simulations of Au Penetration Through Alkanethiol Molecules on the Au(111) Surface

In the second project, the dynamics of Au atoms on alkanethiol monolayers was described using classical molecular dynamics in conjunction with first principles quantum-mechanical calculations. The interaction between the Au atoms and the monolayer was adjusted on the basis of the quantum calculations. The Au atoms were observed to penetrate into the monolayer at room temperature, as in experiments. There was no Au penetration at 50K, which is also in agreement with the experiments. This work has been accepted for publication in the Journal of Physical Chemistry C.

Third Project: Dynamics of Silver Clusters on Alkanethiol Molecules on the Au(111) Surface

In the third project, silver clusters of various sizes were placed on top of the alkanethiol monolayers and their diffusion, dynamics and sintering processes were analyzed. This work has been accepted for publication in Physical Review B.

CHAPTER 2
METHOD

Molecular Dynamics

Molecular dynamics is a virtual experiment that represents an interface between laboratory experiments and theory. It is a form of computer simulation in which the atoms and the molecules are allowed to interact under the laws of physics for a period of time. The molecular dynamics simulates the way large systems behave under various conditions.

Since the 1970s, the method of molecular dynamics has become popular and has been used in physics, chemistry and biology. MD is used to model X-ray crystallography and NMR results to determine protein structures. It is also possible to use the MD in order to describe atomic-level phenomena and to design new nanotechnological devices. In an MD simulation the main parameters are: the potentials to be used, the thermostat, the integration algorithm and the boundary conditions.

Potentials Used

The Universal Force Field (UFF)[44] is used to describe the bonding parameters of organic molecules in our simulations. This force field is based on the element, its hybridization and its connectivity. It is possible to generate the force field parameters for the entire periodic table using various combination rules.

Five-character mnemonic labels are used to describe the atoms. The first two characters are used to denote the chemical symbol. The chemical symbol is described by the first two characters. An underscore is used in the second column if the symbol has one letter. For example hydrogen atom is described as H_ and rhodium as Rh. The next column represents the hybridization or the geometry. (1=linear, 2=trigonal, R=resonant, 3=tetrahedral, 4=square planar 5= trigonal bypyramidial, 6=octahedral) C_3 is used to describe tetrahedral carbon atom.

The potential energy of a molecule is described as the combination of bond-stretching (E_R), bond angle bending (E_θ), dihedral angle torsion (E_υ) and non-bonding interactions (E_{vdw}).

$$E = E_R + E_\theta + E_\upsilon + E_{vdw} \tag{2-1}$$

To describe the bond stretching, UFF[44] uses either the harmonic oscillator function or the Morse function

$$E(r) = \frac{1}{2} k_{ij} \left(r - r_{ij} \right)^2 \qquad \text{Harmonic oscillator} \tag{2-2}$$

$$E(r) = D_{ij} \left[e^{-\alpha \left(r - r_{ij} \right)} - 1 \right]^2 \qquad \text{Morse function} \tag{2-3}$$

k_{ij} is the force constant in units of (kcal/mol)/Å^2, r_{ij} is the natural bond length in Å. D_{ij} is the bond dissociation energy (kcal/mol) and

$$\alpha = \left[\frac{k_{ij}}{2 D_{ij}} \right]^{1/2} \tag{2-4}$$

The second term is the valence angle potential. The valence angle (bending) potential describes the bond bending terms between specified atoms. In this type of force field the angle bend term is described as the harmonic cosine function:[44]

$$U\left(\theta_{ijk} \right) = k/2 \left[\cos\left(\theta_{ijk} \right) - \cos\left(\theta_0 \right) \right]^2 \tag{2-5}$$

where θ_{ijk} is the angle between three atoms and θ_0 is the equilibrium angle.

The third term in the potential is the torsional term, which can be written as follows:[44]

$$U\left(\vartheta_{ijkn}\right) = A\left[1+\cos\left(m\vartheta_{ijkn}-\delta\right)\right] \tag{2-6}$$

where m is the multiplicity and δ is the phase angle.

The last term is the van der Waals term. To describe these interactions a Lennard-Jones type expression is used:[44]

$$E_{vdw} = \left\{-2\left[x_{ij}/x\right]^{6} + \left[x_{ij}/x\right]^{12}\right\} \tag{2-7}$$

In this expression, $x_{ij} = 1/2\left(x_i + x_j\right)$ where x_i is the atomic van der Waals radius and D_{ij} is the potential well depth defined as $D_{ij} = \left(D_i D_j\right)^{1/2}$.

The UFF is commonly used to simulate organic molecules such as alkanethiols,[45] benzenethiols,[46] and it gives a generally accurate description of organic molecules.

The metal-metal bonding interactions are described with the Sutton-Chen potential.[47] This type of potential describes metals very well. This potential combines the long-range interactions (van der Waals terms as the tail) and the short-range interactions. The analytical form of the potential is:[47]

$$V_{ij}\left(r_{ij}\right) = \varepsilon\left(a/r_{ij}\right)^{n} \tag{2-8}$$

$$p_{ij} = \left(a/r_{ij}\right)^{m} \tag{2-9}$$

$$F\left(p_i\right) = -c\varepsilon\sqrt{p_i} \tag{2-10}$$

with parameters ε, a, n, m, c. The term ε is an energy term, a is a term used to describe the length and m and n are integers such that n is greater than m. The typical values of m are between 6 and 8 and for n between 9 and 12 and c is a dimensionless parameter.[47]

This type of potential has been used to describe the metal clusters in various scientific papers.[48-50]

Thermostat

In our simulations the Berendsen thermostat[51] was used to keep the temperature constant. In this type of thermostat, the system is coupled to an external heat bath which is fixed at a desired temperature. This bath acts as a source of thermal energy and supplies or removes heat from the system. The rate of change of temperature is proportional to the difference in temperature between the bath and the system and the velocities are scaled at each step,[51]

$$dT(t)/dt = 1/\tau\left(T_{bath} - T(t)\right) \tag{2-11}$$

In this equation, τ is a coupling parameter that defines how strongly the bath and the system are coupled together. In this type of thermostat, there is an exponential decay of the system towards the desired temperature.[51]

If the coupling factor τ is large, then the coupling will be weak. If this factor is small, the coupling will be strong. The change in temperature between the successive time steps is:

$$\Delta T = \delta t/\tau\left(T_{bath} - T(t)\right) \tag{2-12}$$

The scaling factor for the velocities is:

$$\Lambda^2 = 1 + \delta t/\tau\left(T_{bath}/T(t) - 1\right) \tag{2-13}$$

Verlet Leapfrog Algorithm

With continuous potentials, the motions of all particles are coupled together, giving rise to a many-body problem that can not be solved analytically. Instead the equations of motion are integrated using a *finite difference method.*[52] In this method, continuous potential models are used to generate molecular dynamics trajectories that are pairwise additive. The idea is to break the integration into many small stages, each separated in a fixed time δt. The total force on each particle is the vector sum of its interactions with other particles. By looking at the force, it is possible to determine the acceleration of particles and then these are combined with the position and velocities at time t and then the velocities and positions are calculated at a time $t + \delta t$. During each time step, the force is assumed to be constant. The next step determines the forces at a time $t + 2\delta t$.[52]

Several algorithms can be used to integrate the equations of motion. These algorithms are based on the assumption that the positions and the dynamic properties can be approximated as Taylor series expansion:

$$R(t+\delta t) = r(t) + \delta t v(t) + \tfrac{1}{2}\delta t^2 a(t) + \tfrac{1}{6}\delta t^3 b(t) + \tfrac{1}{24}\delta t^4 c(t) + \ldots \quad (2\text{-}14)$$

$$V(t+\delta t) = v(t) + \delta t a(t) + 1/2\,\delta t^2 b(t) + \tfrac{1}{6}\delta t^3 c(t) + \ldots \quad (2\text{-}15)$$

$$a(t+\delta) = a(t) + \delta t b(t) + 1/2\delta t^2 c(t) + \ldots \quad (2\text{-}16)$$

$$b(t+\delta t) = b(t) + \delta t c(t) + \ldots \quad (2\text{-}17)$$

In these equations, v is the velocity, a is the acceleration and b is the third derivative.[52] One of the most common methods for integrating the equations of motion is the Verlet algorithm.[53] This algorithm uses the positions at time t and the positions from the previous step. $R(t-\delta t)$ to calculate new positions at $t + \delta t$.[53]

$$r(t+\delta t) = r(t) + \delta t v(t) + 1/2\,\delta t^2 a(t) + \ldots \tag{2-18}$$

$$r(t-\delta t) = r(t) - \delta t v(t) + \tfrac{1}{2}\,\delta t^2 a(t) - \ldots \tag{2-19}$$

If these two equations are added and if the difference in positions at times $t+\delta t$ and $t-\delta t$ are divided by $2\delta t$, the velocity is:

$$v(t) = \left[r(t+\delta t) - r(t-\delta t)\right] / 2\delta t \tag{2-20}$$

In our simulations the *leap-frog* algorithm is used.[53, 54] This type of algorithm uses these equations:

$$r(t+\delta t) = r(t) + \delta t v(t + 1/2\delta t) \tag{2-21}$$

$$v\left(t+\tfrac{1}{2}\delta t\right) = v\left(t-\tfrac{1}{2}\delta t\right) + \delta t a(t) \tag{2-22}$$

In this algorithm, the velocities $v\left(t+\tfrac{1}{2}t\right)$ are calculated from the velocities at time $\left(t-\tfrac{1}{2}\delta t\right)$ using the accelerations at time t. The velocities are:

$$v(t) = \tfrac{1}{2}\left\{\left(v(t+\tfrac{1}{2}\delta t\right) + v\left(t-\tfrac{1}{2}\delta t\right)\right\} \tag{2-23}$$

The velocities "leap-frog" over the positions to give their values at $\left(t+\tfrac{1}{2}\delta t\right)$. The positions leap over the velocities to give the values at $(t+\delta t)$ and so on. The advantage of this algorithm is that there is no need to calculate the differences of large numbers.[53, 54]

Periodic Boundary Conditions

Periodic boundary conditions are used to simulate an infinitely tiled system that has one or more macromolecules in a bath of an explicit solvent. When the simulations are performed in a vacuum environment, the molecules will fly away unless there is a restraining force. Another

option would be to use reflective walls, but this introduces unwanted forces into the system, which causes additional complication.

When we apply periodic boundary conditions, we define a *unit cell* to give an infinite description of the system. When a molecule passes through one of the faces of the unit cell, it reappears on the other side of the unit cell with the same velocity. There are various types of periodic boundary conditions such as the cubic boundary condition, orthorhombic boundary condition, slab boundary condition and the parallelepiped boundary condition. The choice of a periodic boundary condition is important. If the periodic box is "too small" then the molecule interacts with its own tail, which will lead to unphysical dynamics. The idea is that, a particle will interact with the closest image of the remaining particles in the system. This is called the *minimum image condition.*

In our molecular dynamics simulations we applied an orthorhombic periodic boundary condition with dimensions of $44.91x43.12x80$ Å to give an infinitely tiled description of our systems.

Density Functional Theory

Density functional theory (DFT) is used to investigate the electronic structure of the ground state of molecules and atoms. This method is used widely in computational physics and chemistry. DFT has also been a useful tool for solid-state calculations and is currently a leading method for electronic structure calculations. However, it is difficult to describe intermolecular interactions, such as van der Waals forces, charge transfer excitations, transition states, potential energy surfaces, and band gaps in semiconductors using DFT. The main idea behind DFT is to replace the many-body electronic wavefunction with the electronic density. In this theory, there are three spatial variables for each of the N electrons and the many-body wavefunction depends on 3N variables.

Hohenberg-Kohn Theorems

DFT is based on the Hohenberg-Kohn Theorems.[55] According to these theorems, there is a one-to-one mapping between the ground state electron density and the ground state wavefunction of a many-particle system. These theorems also state that the ground state density minimizes the total electronic energy of the system. These theorems are true only for the ground state in the absence of external fields.[56]

Formalism of DFT

The Kohn-Sham equations are a set of eigenvalue equations within density functional theory (DFT).[57] DFT reduces a many-body problem for the N particle wavefunction $\psi(r_1, s_1;....; r_N, s_N)$ to one in terms of the charge density $p(r)$ using the Hohenberg-Kohn theorems.[55] The wavefunction has 4N variables and the charge density has 3 variables. It is possible to write the total energy as a functional of the charge density:

$$E[p] = T[p] + \int V_{ext}(r)p(r)dr + V_H[p] + E_{XC}[p] \tag{2-24}$$

where T is the kinetic energy of the system and V_{ext} is the external potential acting on the system. The term $V_{H,}$

$$V_H = \frac{e^2}{2}\int \frac{p(r)p(r')}{|r-r'|}drdr' \tag{2-25}$$

is the Hartree energy and the E_{xc} is the exchange correlation energy. It is difficult to obtain the exchange energy exactly, and so it is approximated. The kinetic energy is usually formulated in terms of charge density. It is possible to formulate the charge density as the sum of squares of orthonormal wave functions $\psi_i(r,s)$:

$$p(r) = \sum_{i}^{N} \sum_{s} \left| \psi_i \ (r,s) \right|^2 \tag{2-26}$$

which as solutions to the Schrödinger equation for N electrons in an effective potential $V_{eff}(r)$,

$$-\frac{\hbar^2}{2m}\nabla^2 \psi_i(r,s) + \upsilon_{eff}(r)\psi_i(r,s) = \varepsilon_i \psi_i(r,s) \tag{2-27}$$

The effective potential is:

$$\upsilon_{eff}(r) = V_{ext}(r) + e\int \frac{p(r')}{|r-r'|}dr' + \frac{\delta E_{xc}[p]}{\delta p} \tag{2-28}$$

Combining these equations, we get the Kohn-Sham orbital equations that are solved iteratively until a self-consistency is reached. The total energy of the system is:

$$E = \sum_{i}^{N} \varepsilon_i - V_H[p] + E_{XC}[p] - \int \frac{\delta E_{xc}[p]}{\delta p(r)} p(r) dr \tag{2-29}$$

In DFT calculations, the idea is to find single particle solutions to the Kohn-Sham equation:

$$\left(\nabla^2 + V_{eff}\right)\left|\psi_i\right\rangle = \varepsilon_i \left|\psi_i\right\rangle \tag{2-30}$$

The single particle orbitals can be represented in any complete basis set. In VASP,[57, 58] the basis sets are plane waves that can be written in the following form:

$$\psi_k(r) = \sum_{G} c_{k,G} e^{i(G+k).r} \tag{2-31}$$

The Gs are reciprocal lattice vectors and k is a symmetry label in the First Brillouin zone. We used the VASP[58, 59] code to perform our quantum-mechanical calculations. VASP is a complex package to perform quantum-mechanical calculations using pseudopotentials. Pseudopotentials are used to replace the effects of the motions of core electrons in an atom and its nucleus with an effective potential, or pseudopotential. Instead of a Coulombic potential term

for the core electrons there will be a modified effective potential term which is the pseudopotential.

In our simulations we used the "projector augmented wave method" (PAW)[60] and the PW91[61] exchange correlation functional. In all calculations, with a cutoff energy of 300 eV was used. In the VASP code, the cut-off energy for a plane wave basis set is given in eV. All plane waves with a kinetic energy smaller that E_{cut}.

$$\frac{(G+k)^2}{2} \leq E_{cut} \tag{2-32}$$

The choice of cutoff energy depends on the elements in the system. The energy decreases to the ground state energy as E_{cut} increases. We used 4x4x1 k-point Monkhorst-Pack[62] grid. A Monkhorst-Pack grid is a method to choose a set of k-points for sampling the Brillouin zone. It is a rectangular grid of points of dimensions $M_X \times M_y \times M_z$, spaced evenly throughout the Brillouin zone. As we increase the size of the dimensions of the grid, we get a finer and a more accurate sampling of the zone. In our simulations, Methfessel Paxton[63] smearing is used due to the presence of Au metal in our systems.

Density of States

The density of states (DOS) is a property that shows how closely-packed the energy levels are in a quantum-mechanical system. The symbols g, p, n, N are used to describe the density of states, where $g(E)$ is a function of the internal energy E. The expression $g(E)dE$ represents the number of states between the energy E and the energy $E + dE$. DOS refers to electron, photon and phonon energy levels in a crystalline solid and is widely used in condensed matter physics. A DOS of zero means the electrons can not be excited to that energy.

In the VASP[58, 59] code, it is possible to calculate the DOS in units of *number of states/unit cell*. The density of states (DOS) n, is determined by the difference of the integrated DOS between two points.

$$n(\varepsilon_i) = \left(N(\varepsilon_i) - N(\varepsilon_{i-1})\right) \Big/ \Delta\varepsilon \tag{2-33}$$

where $\Delta\varepsilon$ is the distance between two pins (energy difference between two grid points) and $N(\varepsilon_i)$ is the integrated DOS,

$$N(\varepsilon_i) = \int_{-\infty}^{\varepsilon_i} n(\varepsilon) d\varepsilon \tag{2-34}$$

VASP[58, 59] also gives the projected DOS on different orbitals (s,p,d) for each individual atom in the system. It is possible to sum the PDOS and get the total DOS for one component of the entire system. The integration of the total DOS up to the Fermi energy level E_F gives the total number of electrons in the system. It is also possible to calculate the number of electrons for each component of the system (integration up to E_F) after summing the PDOS for all the atoms comprising this component. These techniques are helpful in charge analysis.

CHAPTER 3
MOLECULAR DYNAMICS SIMULATIONS OF ALKANETHIOL MONOLAYERS WITH AZOBENZENE MOLECULES ON THE AU (111) SURFACE

Introduction

The concept of using molecules as components in electronic circuits was proposed theoretically in the early 1970s.[64] The first experimental confirmation of this idea was achieved nearly 20 years later. Following the measurement of the conductance of a single molecule by the Reed group,[65] a variety of molecules has now been proposed as candidates for molecular devices.[66-72] Prominent among these are azobenzene and its derivatives.

One feature that makes azobenzene appealing as a molecular device is its photochemistry. Molecules in this family can be transformed between their *cis*- and *trans*- isomers via optical excitation. This makes them potential candidates as optical switches, or other nano-optomechanical devices.[73, 74] Recent theoretical work indicates that the conductance of the two conformations differs by a factor of 100.[75] This raises the possibility that azobenzene derivatives can be used as the ON and OFF states of a single-molecule, light-driven switch. Experimental studies in several groups have confirmed this idea, via direct measurement of conductance with a scanning tunneling microscopy (STM) tip.[76, 77]

For azobenzene, or any other molecule, to be useful as a device, it must be attached in some way to the solid state, ideally to metallic leads. As a first step towards this goal, candidate molecules can be studied in self-assembled monolayers (SAMs), which help to stabilize them and constrain their geometry. Indeed, SAMs are proving to be essential components of emerging bottom-up technology.[78-80] Understanding the properties of these monolayers, and how these properties are altered by the addition of guest molecules is critical to progress in the field.

Many polymer/organic molecule assemblies have been investigated recently, due to their vast range of applications as protective coatings, in surface chemistry, and as bio-sensors.[2, 5, 81] In

particular, SAMs of alkanethiol on the Au(111) surface are structurally simple, thermodynamically stable, and have well-defined order. As a result, their structure and growth have been studied extensively since their discovery in the early 1980s.[1, 82-87] Monolayers on surfaces can be used as host matrices to support guest molecules for studies of the properties of the guest molecules, or to stabilize metallic nano-crystals.[88] Such systems provide a fertile test bed for investigating the properties of molecular electronics devices.

In the laboratory, molecules are often assembled as monolayers on a solid surface or inserted into alkanethiol SAMs and studied using scanning tunneling microscopy (STM).[89, 90] In the former case, the STM tip is usually in contact with several molecules during the measurement. In the latter, the interaction between the host alkanethiol molecules and the guest molecule can influence the packing structure of the monolayer. In general, the structure of a monolayer mixed with guest molecules will have large local disorder, even if the monolayer itself is highly ordered. Since conductance is sensitive to the contact between the STM tip and the molecules of interest, a clear physical picture of the structure, thermodynamics and dynamics of the system is essential. Simulations are especially valuable in this regard, since information concerning the microscopic details of a heterogeneous structure is often difficult to obtain directly in experiments.

One example of the diverse phenomena associated with SAMs, which must be incorporated into the design of potential molecular devices, is the phase transition of the quasi two-dimensional system as a function of temperature. Beginning with the first experimental evidence[91] for this transition, substantial effort has been devoted to preparing true two-dimensional systems and to properly characterizing the transition. On the theory side, molecular dynamics simulations have played a significant role since the 1960s. Systems such as SAMs of chain-shaped polymers or peptides are much more complex than ideal, monoatomic 2D systems, which leads to exotic

behavior and rich physics during phase transitions. For a pure alkanethiol monolayer on a gold surface, which is the reference system for our work, a number of groups have reported investigations of the structure and characteristics of the phase transition. In addition to STM,[92] experimental techniques such as low-energy atom diffraction[93] (LEAD), grazing-incidence x-ray diffraction (GIXD),[94] and atomic force microscopy (AFM)[95] have been used to investigate the structure of alkanethiol molecules on the Au(111) substrate. These studies have reported tilt angles of the alkanethiol chains, temperature effects, and the coverage and the chain length dependence of the properties of the monolayers.

A general review on properties and issues of SAMs has been reported by Ulman.[2] Pioneering theoretical molecular dynamics (MD) simulations were provided by Klein's group,[38, 39] in which the surface was modeled with a structureless model potential. Zhang and Beck[96] used a consistent valence force field to describe the molecular systems. Leng *et al*.[46] and L. Zhang *et al*.[97]calculated properties of the monolayer using a similar model. In papers by Bhatia and Garrison,[41, 42] a united-atom model was used to describe the molecular potentials and an MD/MC-corrected effective medium (MD/MC-CEM) potential was used to describe the Au surface. Beardmore[43] developed an empirical potential function by fitting parameters of the Au-S interaction to quantum calculations. Finally, Fisher *et al*.[98] reported structural results using a hybrid quantum mechanical and molecular mechanical (QM/MM) method.

Inspired by the developments in the above-mentioned scientific pursuits, we have performed molecular dynamics simulations to study pure and azobenzene-containing alkanethiol monolayers on the Au(111) surface. We address such issues as the structure of the monolayer and its temperature dependence, as well as the caloric curve, heat capacity, phases and phase transitions of the quasi-two dimensional systems. Our focus is a comparison of the pure and mixed

systems, as well as on local distortions of the alkanethiol monolayer when guest molecules are introduced. Our aim in this is to provide detailed information for future applications of azobenzene and similar systems as molecular devices. The chapter is organized as follows: Section II describes the system and the MD models; Section III presents results; and Section IV contains a summary.

Systems, Simulation Model, and Computational Details

This work begins by the design of models for three monolayers. These include systems comprising a pure dodecanethiol layer, a dodecanethiol monolayer containing a *trans*-azobenze molecule, and a dodecanethiol monolayer containing a *cis*-azobenzene molecule. Note that the species we refer to as "azobenzene" (See Fig. 3.1) have been chemically substituted with a terminal CH_2S group, to form the S-Au bonds to the surface, and a terminal CH_2SH group on the end directed away from the surface. The proper name of this molecule is (bis-[4-methanethiol-phenyl] diazene, but we will refer to it as "azobenzene" for simplicity. Similarly, although all of the results in this paper were obtained for dodecanethiol, a 12-carbon alkanethiol, we will refer to this system as simply "alkanethiol".

The monolayers are placed on the (111) surface of 6- and 9-layer Au slabs. In the lateral direction, each layer of the surface contains 18x15=270 atoms, with a size of 44.9 Å by 43.2 Å. For the homogeneous system, ninety dodecanethiol molecules are included to simulate 100% coverage of the surface. Periodic boundary conditions are used in all three directions. A 20 Å vacuum is inserted between two adjacent slabs in the z-direction to model the (111) surface. The MD unit box has the shape of a hexagonal $(\sqrt{3}\times\sqrt{3})$R30 lattice in the *x* and *y* directions.

All-atom potential functions are used with a Dreiding force field[99] to describe the intra-and inter-molecular interactions for all molecules in the three systems. We have performed substantial tests of various potentials, including the parameters used by Jung *et al.*[100] to describe

benzenethiolate and benzyl mercaptide on Au(111) in MD simulations. We found, though, as illustrated below, that for this work the potentials developed by Sellers, et al.[8] were the most convenient and accurate. The two-body Lennard-Jones potentials for Au-S were developed from a simple Au-S harmonic function.[8] The parameters were ε = 0.3 eV and σ = 2 Å.

We chose the Universal Force Field (UFF)[44] to describe the van der Waals interactions, and modeled the interactions between Au atoms by the Sutton-Chen Potential.[47, 101] In previous approaches, the interface between the Au surface and monolayer included: (i) Two-body Lennard-Jones potentials for S and Au; (ii) Three-body truncated harmonic potentials for C, S and Au; and (iii) van der Waals interactions between Au atoms and C, H and S. Details of the potentials used in our simulations are discussed below.

Before embedding the *cis*- and *trans*- azobenzene into the alkanethiol monolayer, energy minimization was performed with the Dreiding force field. We found that the *trans*- structure is about 0.7 eV lower than the energy of the *cis*- structure, which is close to the value of 0.6 eV determined by high-level quantum calculations[75] and experiments.[102] The pure monolayer was also optimized before dynamical simulation. The heterogeneous systems were prepared by removing three (for the *trans*-azobenzene) or four (for the *cis*-azobenzene) dodecanethiol molecules from the pure system, and inserting an azobenzene molecule in the resulting cavity.

At each temperature, we ran MD for 400 ps with a 2.0 fs time step before recording statistical information. The Berendsen thermostat[51] was used to control the temperature. The systems were held at constant number, volume, and temperature (NVT ensemble). After relaxation at 0 K, all three systems were heated from 50 K to 800 K with an interval of 50 K. After equilibration, the MD runs continued for 240 ps, and structures were saved every 200-400 steps. To eliminate possible complications caused by *cis*- to- *trans*-transitions of the azobenzene during

high temperature simulations, the C-N=N-C dihedral angles were fixed at temperatures higher than 400 K.

Results

Tests of Molecule-Surface Potentials, 0 K Structures

The first simulation performed energy minimization using potential parameters from the work of Jung *et al*.[100] Figure 2 depicts the optimized structure at 0 K. With this potential, we found that the first three layers reconstructed. In the initial structure, the S atoms in the dodecanethiols are surrounded by three Au atoms in the first layer (Fig.2a), but in the reconstructed structure, each S atom has six nearest-neighbor Au atoms (Fig.2b). In addition, some of the Au atoms in the second layer move upward from their initial positions (Fig. 2c). This reconstruction would be expected to have a dramatic effect on the structure and energetics of the monolayer. The question, though, is whether the reconstruction is real, or an artifact of the potentials.

To understand the effects on the structure due to the three-body potential, we calculated the energy of a single dodecanethiol molecule at a distance from the surface of 5 Å to 2 Å in steps of 0.2 Å. At each step, a single-point energy (static energy) was obtained. We found that the adsorption energy of the optimal structure is about 3.91 eV (90 kcal/mol) at the lowest-energy point (1.8 Å above the first surface layer). As the system relaxes, this binding energy would be expected to increase to a value considerably higher than the experimental value of 1.3 eV/molecule for this monolayer.[5] A new set of two-body potential parameters was tested to reduce the binding energy to 1/3 of its original value. Once again, however, surface reconstruction occurred. We conclude from these tests that the two-body potential does not cause the reconstruction.

We next examined the role of the 3-body potential in the surface reconstruction. The 3-body potential, which is a truncated harmonic potential, depends on three Au-S-C angles, as shown

in Fig. 3a. Before optimization, the three Au-S-C angles are set to $\theta_1 = \theta_2 = 114°$, and $\theta_3 = 173^o$ (due to the all-*trans* structure assumed for dodecanethiol). This structure is nearly 3.0 eV higher than the energy of the equilibrium structure. Consequently, the force generated by this strong potential energy pushes the Au atoms away from the slab, and causes the surface to reconstruct. When the strength of the 3-body potential is adjusted, a variety of interface structures are formed. Fig. 3-3b shows a structure in which an S atom of an alkanethiol has been moved from its initial hcp hollow site to a bridge-fcc site to reduce the overall 3-body energy.

To investigate the suspicious surface reconstruction and Au-Au elongation further, studies of a smaller model system were performed using density functional theory (DFT).[57] The calculations used the Vienna Atomic Simulation Package (VASP),[58, 59] with the projector augmented wave method (PAW)[60] and the Perdew, Burke and Ernzerhof (PBE)[103] exchange correlation functional. We considered a monolayer of CH_3S on the Au(111) surface. The unit cell chosen was five-layers thick in the *z*-direction and contained 3 Au atoms per layer, for a total of 15 Au atoms.

Three different initial configurations of CH_3S on the Au(111) surface were modeled. One corresponds to the CH_3S on the fcc hollow site, the second is on the hcp hollow site, and the third is the reconstructed structure. After ionic relaxation using DFT, we found that the energy of the configuration in which the molecules are on the fcc site is 0.1 eV lower than that on the hcp site, which is in good agreement with previous quantum calculations.[104] In contrast, the reconstructed structure is unstable, and the system reverts to the non-reconstructed geometry (Fig. 4) when optimized. The results of these quantum calculations provide strong evidence that the reconstructed surface is an artifact due to imperfect potential functions.

To provide further detail about the Au-Au elongation, additional (DFT)[57] calculations were performed using a $(\sqrt{3}\times\sqrt{3})$R30 surface unit cell. The slab included 5 atomic layers of Au and the bottom 2 layers were frozen during ionic relaxation. We used the theoretical value of 4.17 Å for the Au fcc lattice constant. The vacuum thickness was at least 15 Å, and the kinetic energy cutoff was 400 eV. We chose a 4x4x1 k-point mesh with Methfessel-Paxton smearing[63] of 0.4 eV were used. The total energy was converged to 2.0 meV/atom with respect to k-point mesh and vacuum thickness. The absolute value of the force on each atom was reduced below 0.02 eV/A at the end of ionic relaxation.

We found that the elongation of the in-plane Au-Au distance for the fcc site upon the methylthiolate adsorption was more than 8% (from 2.95 to 3.20 Å). Gronbeck and Andreoni[105] used a larger surface unit cell of (5x5), corresponding to low coverage, which led to a larger relaxation.

The purpose of this DFT calculations was not to search thoroughly for all possible surface reconstructions induced by methylthiolate adsorption, but to verify whether or not the particular surface reconstruction observed in MD simulations was physical. For this reason, the DFT calculations were performed for the same unit cell of $(\sqrt{3}\times\sqrt{3})$R30, used in the MD calculations. If a larger surface unit cell were used, other surface reconstructions might be observed, as shown recently by Mazzarello, et al.[106]

After analyzing these potentials and their effects on surface construction, we removed the three-body term obtained from Sellers, et al.[8] The gold atoms were held rigid in the production MD simulations. Consequently, the only interaction between the gold surface and the monolayers was the two-body L-J potential obtained from Sellers, et al.,[8] as described above. With these potential parameters, the optimal binding is found to be on an off-center hcp-bridge site, which

agrees with the results of Fisher, et al. using a hybrid quantum-classical model.[98] Figure 5a depicts the energy landscape, as calculated with the empirical potentials, as the molecule moves from site to site on the surface. The various sites on the surface are illustrated in Fig. 5b. Note that the diffusion barrier between the hcp sites and the fcc sites is quite low, which indicates that the dodecanethiol molecules will diffuse rapidly upon thermal excitation. Similar barrier heights have been calculated previously.[43]

Phase Transitions

To study the effects of temperature on the structure and thermodynamics of the monolayers, dynamics simulations were performed within the canonical NVT ensemble. Temperature control was achieved using the Berendsen[51] thermostat for equilibrium states and dynamics. Starting from optimized zero- temperature structures, the three systems were investigated from 50 K to 800 K at intervals of 50 K. After equilibration, statistical data were recorded every 200-400 steps and averaged over 240 ps.

The heterogeneous systems were created initially by removing three alkanethiol molecules from the pure monolayer, and replacing them with a *cis*- or *trans*-azobenzene. We discovered, however, that the *cis*- molecule isomerized to the *trans*- at temperatures above 100 K. This is probably because the *cis*- isomer occupies more space in the plane of the surface than the *trans*-, and hence has greater interactions with the alkanethiol units. To provide additional space, and to reduce the interaction strength, we removed a fourth alkanethiol for the *cis*- isomer simulations. In this case, the *cis*-azobenzene remains stable to thermal isomerizaton at temperatures up to 400 K (note that in the gas phase, *cis*-azobenzene isomerizes thermally at room temperature). At temperatures above 400 K, we fixed the dihedral angles to prevent isomerization of the *cis*- isomer.

Caloric Curves and Heat Capacity. Figure 6 depicts caloric curves (upper panels) and heat capacity C_v (lower panels) for all three systems. The heat capacity is calculated from the energy fluctuations as,

$$C_V = \frac{\left\langle H^2 \right\rangle - \left\langle H \right\rangle^2}{k_B T^2} \quad , \tag{3-1}$$

where H the Hamiltonian, k_B is the Boltzmann constant, and T is the temperature. Strong peaks are seen around 350 K in the C_V curves, indicating a phase transition. Experiments[107] indicate that the phase transition occurs at about 50^0 C (325 K), and thus our calculations are in good agreement with the experiments.

Molecular Orientation. As the temperature increases, molecules in the systems display increased thermal motion. This causes changes in physical properties of the monolayer such as structure and dynamics. Figure 7 presents snapshots from the dynamics to illustrate the structures of the three systems at 50 K, a temperature below the phase transition, and at 350 K, the temperature of the phase transition. One striking feature that can be observed in the figure is the relative orientation of the molecules. At room temperature the dodecanethiol molecules are tilted with similar tilt angles. In the systems with the azobenzene molecules, the dodecanethiol molecules near the azobenzene molecule are disordered only slightly compared to the pure system, and the azobenzene molecule tilts in the same direction as the alkanethiol monolayer (a more quantitative analysis is presented below). At temperatures above the transition temperature, all molecules are oriented normal to the surface including the azobenzene.

To obtain statistical information on the tilt angle, we collected structures along the trajectory and averaged over 240 ps. The tilt angle is defined in Fig. 3-8a. At room temperature,

the experimental value[108] of the tilt angle is 33.7 ± 0.8 degrees. Our simulations predict an average tilt angle of 35.0 ± 5.0 degrees. The distributions of tilt angles are presented in Fig. 3-8b for the pure, *cis*-containing, and *trans*-containing monolayers at three different temperatures. At low temperature (top), all distributions display small deviations from the mean. However, in the heterogeneous systems, the distribution is slightly broader. The results for the thermal behavior indicate that the presence of even a single azobenzene molecule introduces considerable local disorder. This is due, in part, to the density of the monolayer. For the pure system with full coverage, the molecule number density is 1/21.6 $Å^2$; for the *trans*-containing monolayer, it decreases to 1/22.0 $Å^2$; and for *cis*-containing monolayer it decreases to 1/22.3 $Å^2$. The lower density evidently provides more space for the molecule to move and tilt. Note that entropy is proportional to the volume, in general, so these results are not unexpected. As discussed above, the *cis*-isomer would be expected to cause more local disorder than the *trans*-isomer. Note, too, that even with a fourth alkanethiol removed, the distribution of tilt angles is nearly as broad for the *cis*-case as it is for the *trans*-. Figure 3-8b illustrates that the melting begins at 350 K (middle) and is nearly complete by 375 K (bottom), at which point almost all of the molecules are vertical.

Radial Distribution Functions (RDF). Figure 3-9a depicts S-S RDFs for all three systems at three temperatures. As a reference, we consider only the S atoms of the alkanethiol molecules. At low temperature (top), the peaks are quite sharp. Due to the stronger thermal motion at 350 K (middle), the peaks in the RDF curves broaden. At temperatures above the phase transition (bottom), additional broadening is observed. Figure 3-9b displays a snapshot of the positions of the S atoms on the surface at 50 K (top) and 400 K (bottom). Considerable disorder in the structure is evident at the higher temperature.

Surface Diffusion. The dynamical property of surface diffusion provides additional information concerning the physical phase of the monolayers. We have computed the mean square displacement (MSD), $\Delta = \left\langle \left(R(t) - R(0) \right)^2 \right\rangle$, and the diffusion coefficient, $D = \Delta/(4*t)$ as $t \to \infty$, for S atoms on the Au(111) surface as a function of temperature. At low temperature, all three systems are in a solid-like state, with a MSD that is nearly flat (Fig 3-10a). As the temperature increases, the S atoms begin to move from their original locations, and finite (non-zero) slopes are observed. The diffusion constants, which are proportional to the slope of the mean square displacement, are presented in Fig. 3-10b. Above the phase transition, the diffusion constants increase rapidly as the temperature increases. The systems change from solid-like states to liquid-like states. For the two heterogeneous systems, we find that the guest azobenzene molecule enhances the rate of diffusion slightly.

Local Disorder. To quantify the local disorder, which is difficult to achieve in the laboratory, we compute the tilt angle and height of the molecules in the monolayer as a function of distance from the guest azobenzene molecule. For the pure monolayer the center alkanthiol was considered as the reference. Figure 3-11a shows the tilt angles of the molecules as a function of the distance from the guest azobenzene molecule. Figure 3-11b shows the height of the molecules as a function of the distance from the reference azobenzene molecule and the Fig. 3-11c shows a histogram of the height of the molecules at different temperatures. Clear indications of local disorder caused by the guest molecules are evident, although the differences between the *cis*- and *trans*- azobenzene are small

Conclusions

In this chapter, we investigated a homogeneous alkanethiol monolayer and two heterogeneous systems consisting of an alkanethiol monolayer with a *cis*- and *trans*- azobenzene

on the Au(111) surface, using classical molecular dynamics. We found, in agreement with experiment, that at a temperature of about 350 K, the three systems undergo a phase transition from an ordered, tilted structure to a vertical, liquid-like structure. We presented a thorough analysis of temperature-dependent properties such as energy, heat capacity, molecular orientation, radial distribution functions, diffusion, and local disorder. The variations in the properties indicate that the phase transition is first-order for these quasi-two dimensional systems. The global properties of the system, such as the nature of the phase transition, diffusion constants, radial distributions, and the transition temperature are not affected strongly by the guest molecules with the ratio of azobenzene to alkanethiol molecules (1:87 or 1:86) used in the simulations. The local structure of the monolayer, however, is influenced by both the *cis*- and *trans*- azobenzene as indicated by quantities such as the molecular height, and fluctuations in the tilt angle. Further investigations of coverage dependence, monolayers of pure *cis*- and *trans*-azobenzene, and the effects of surface phonons are underway.

A

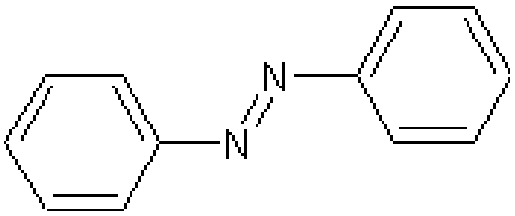

B

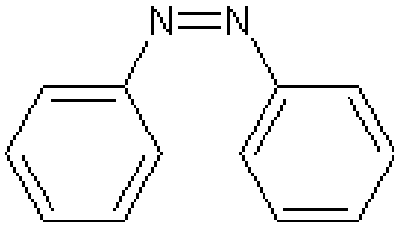

Figure 3-1. Azobenzene molecule. A) *Trans*- azobenzene, B) *cis*- azobenzene

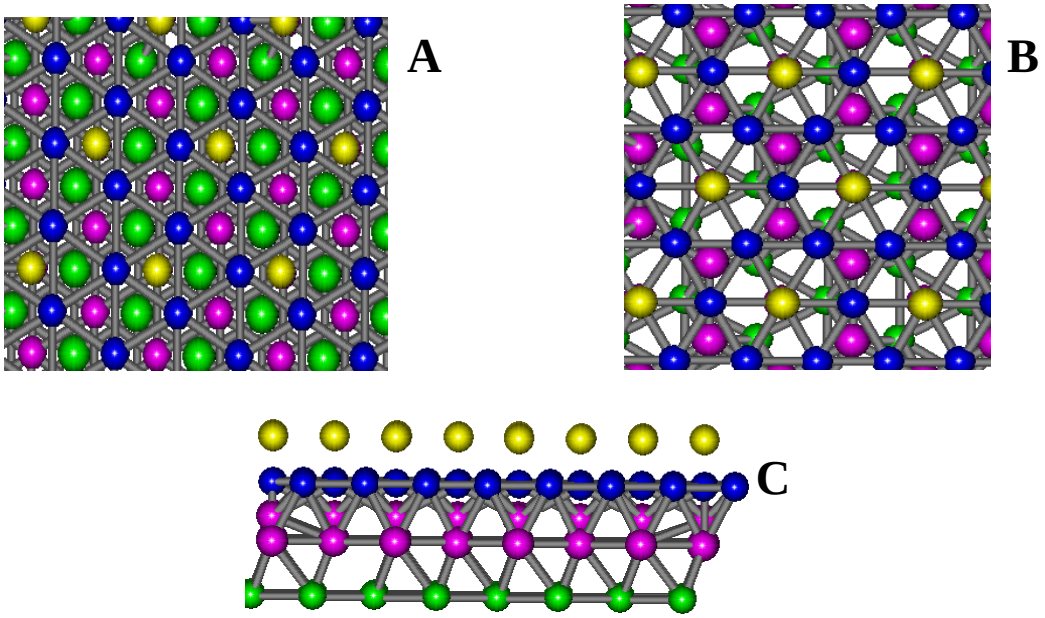

Figure 3-2. Surface structures. A) Top view and side view of the initial Au(111) surface (top 3 layers) including the positions of the S atoms on the alkanethiol molecules. Atoms in yellow are S, while blue, magenta, and green indicate the first, second and third layers of Au, respectively, B) Top view of the reconstructed Au(111) surface (top 3 layers) including the S atoms from azobenzene, C) Side view of the reconstructed structure; S atoms are in yellow, the first layer of gold is blue, the second layer is pink, and the third layer is green.

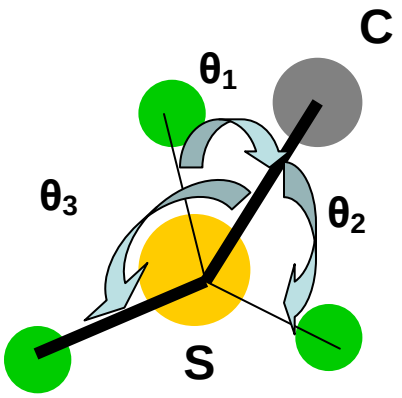

A

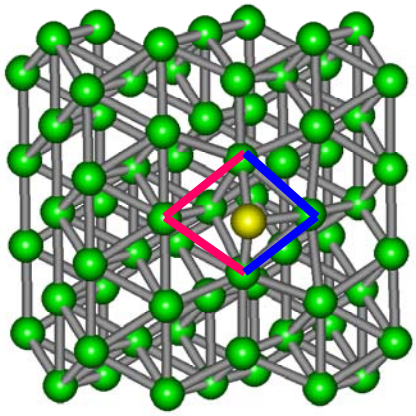

B

Figure 3-3. Au-S-C angles. A) Schematic showing the three Au-S-C angles discussed in the text, B) Adjustment of the 3-body potential parameters produces a variety of interface structures. The center of the left triangle is an hcp hollow site, and the center of the right triangle is an fcc hollow site. The S atom (yellow) is on a bridge-fcc site.

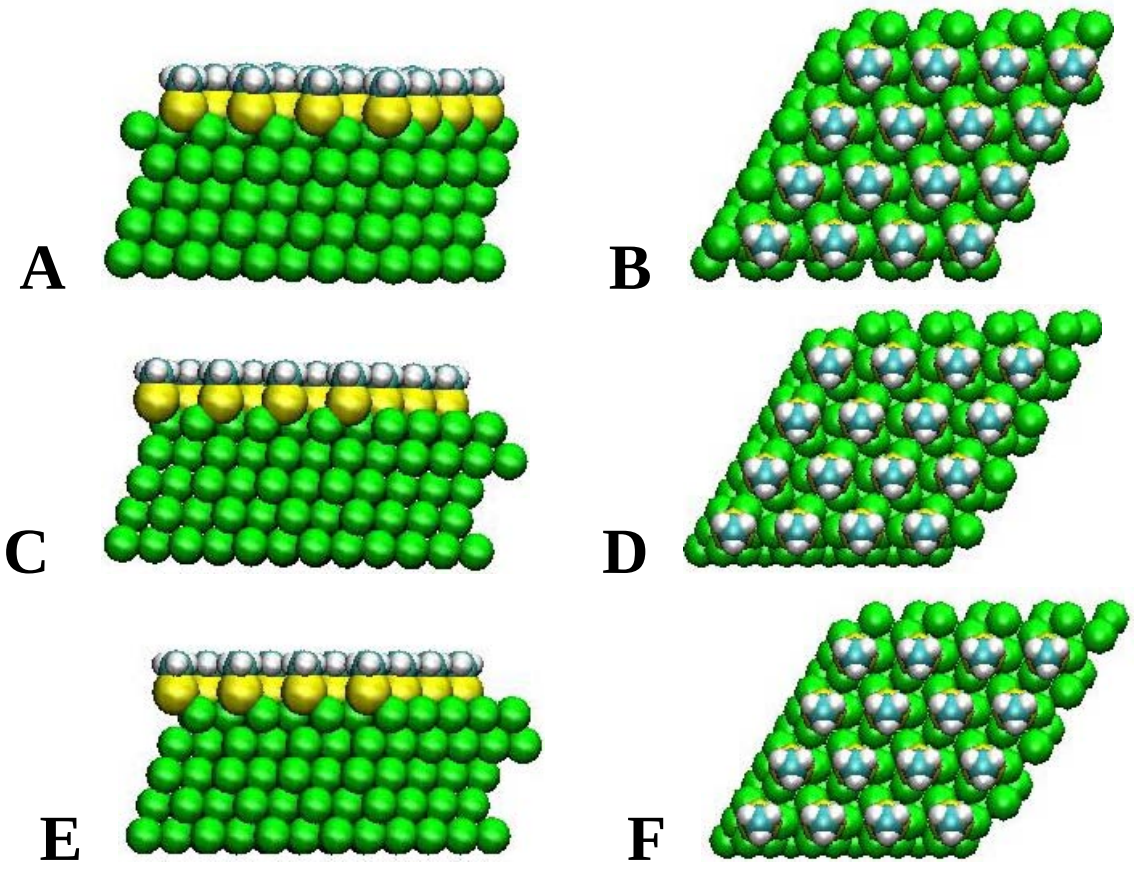

Figure 3-4. CH_3S monolayer on the Au(111) surface (4x4 unit cell). A) and B) CH_3S on fcc hollow sites (top view and side view), C) and D) CH_3S on hcp hollow sites, E) and F) CH_3S on the reconstructed surface.

A

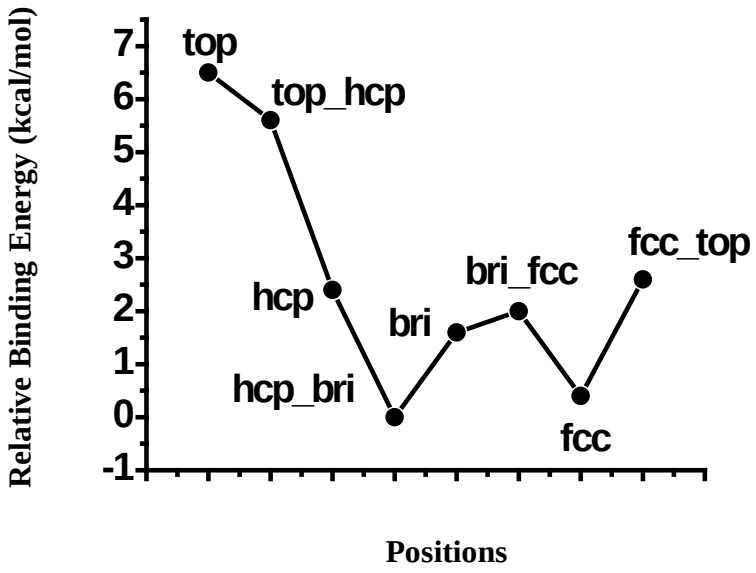

B

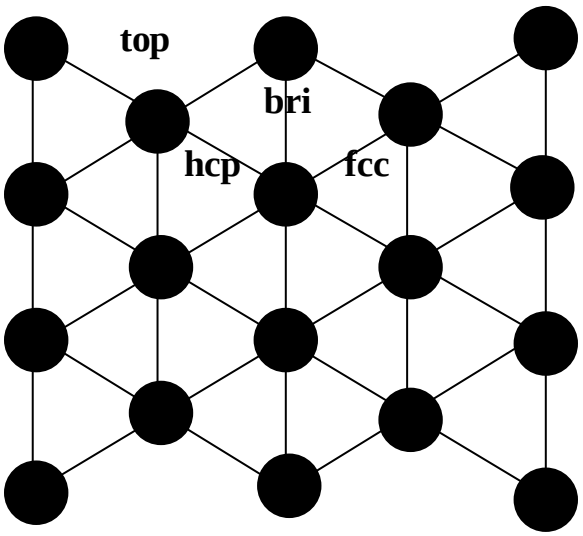

Figure 3-5. Different atomic sites and energy curve. A) Relative binding energy of one dodecanethiol molecule on the Au(111) surface along a selected diffusion path, B) Schematic of the surface, indicating the various surface sites.

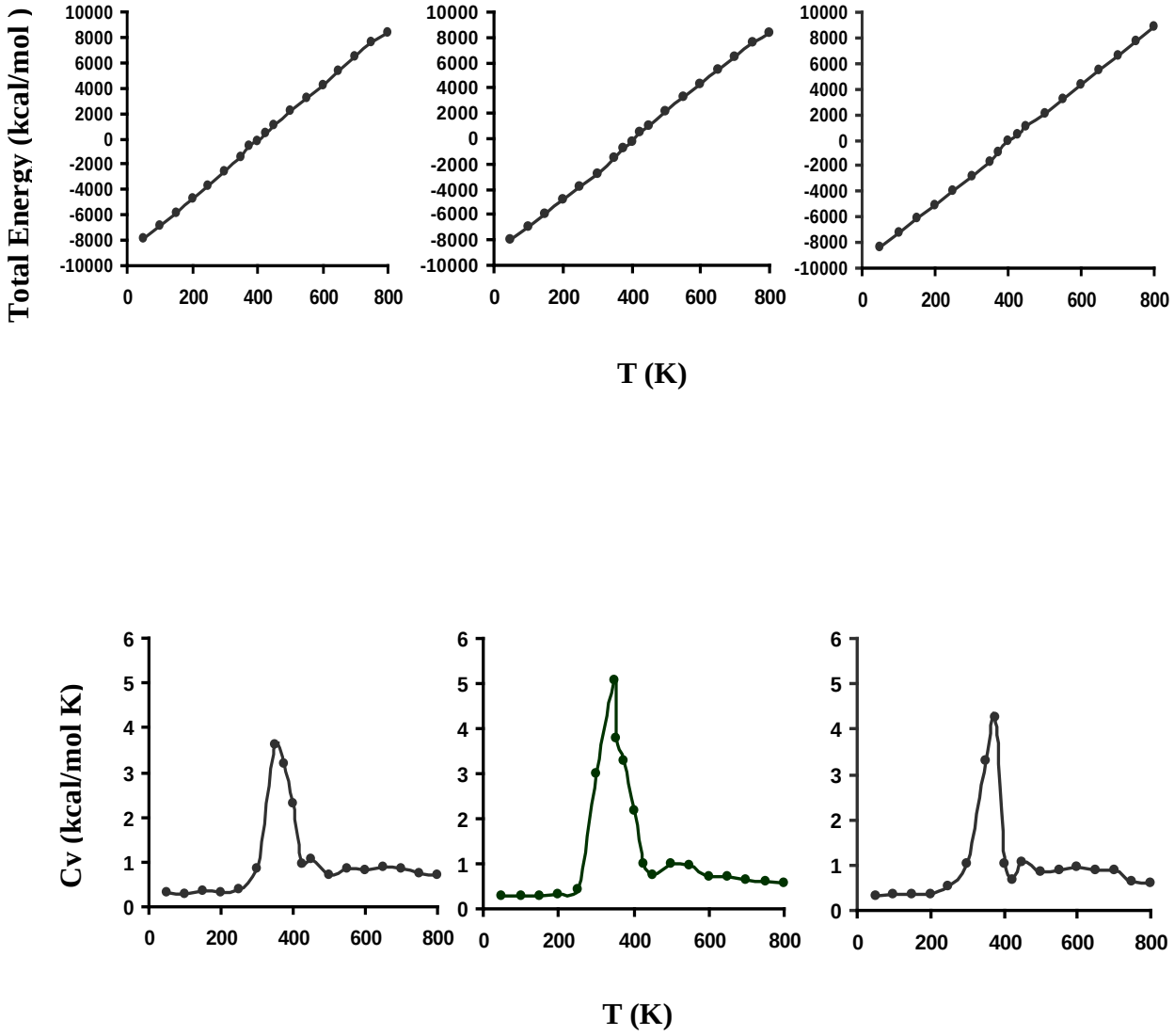

Figure 3-6. Caloric curves. From left to right, are alkanethiol monolayers with the *cis*-containing monolayer, the *trans*-containing monolayer and the pure monolayer. Top: Total energy versus temperature; Bottom: Heat capacity versus temperature.

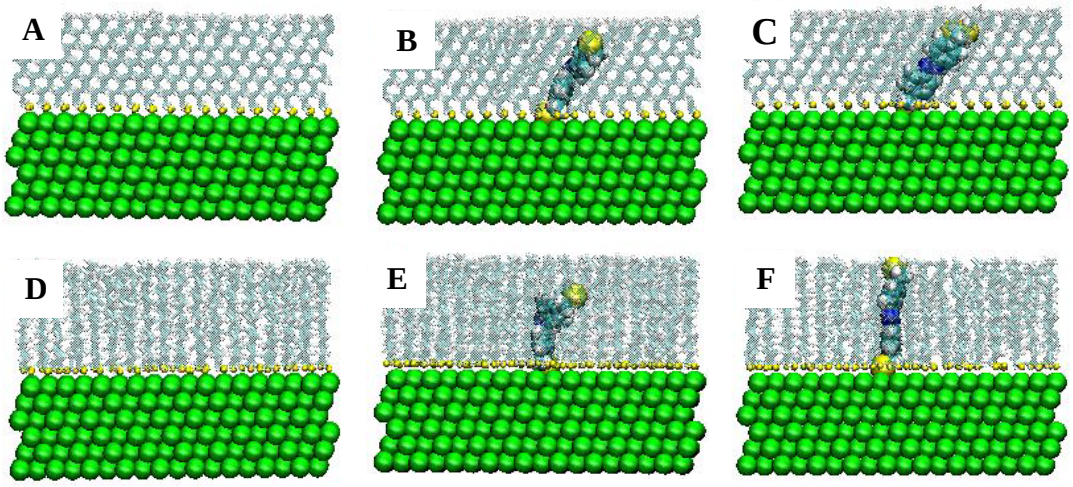

Figure 3-7. Equilibrium configuration of the pure alkanethiol monolayer. The *cis*-containing monolayer and the *trans*-containing monolayer, are on the left and right, respectively. Top: Panels A), B) and C) illustrate the structure at a temperature below the phase transition (50 K); Bottom: D), E) and F) illustrate the structure at the phase transition temperature (350).

A

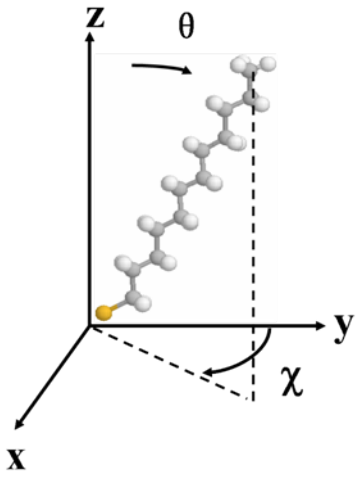

Figure 3-8. Tilt angle. A) Definition of the tilt angle, θ, B) Total distribution of tilt angles. From left to right are the *cis*-containing monolayer, the *trans*-containing monolayer, and the pure monolayer; from top to bottom, 50 K, 350 K, and 375 K.

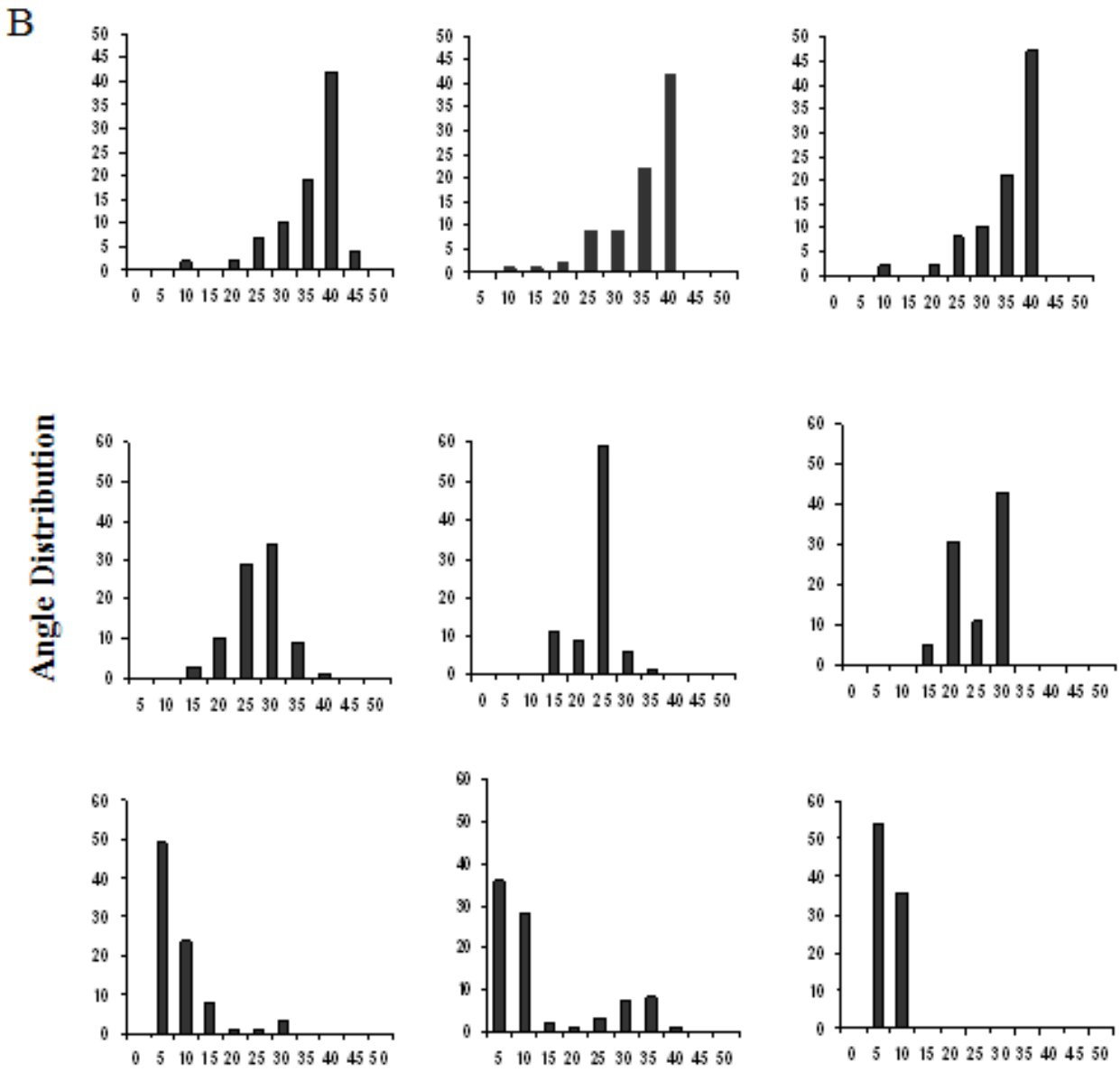

Figure 3-8. Continue

A

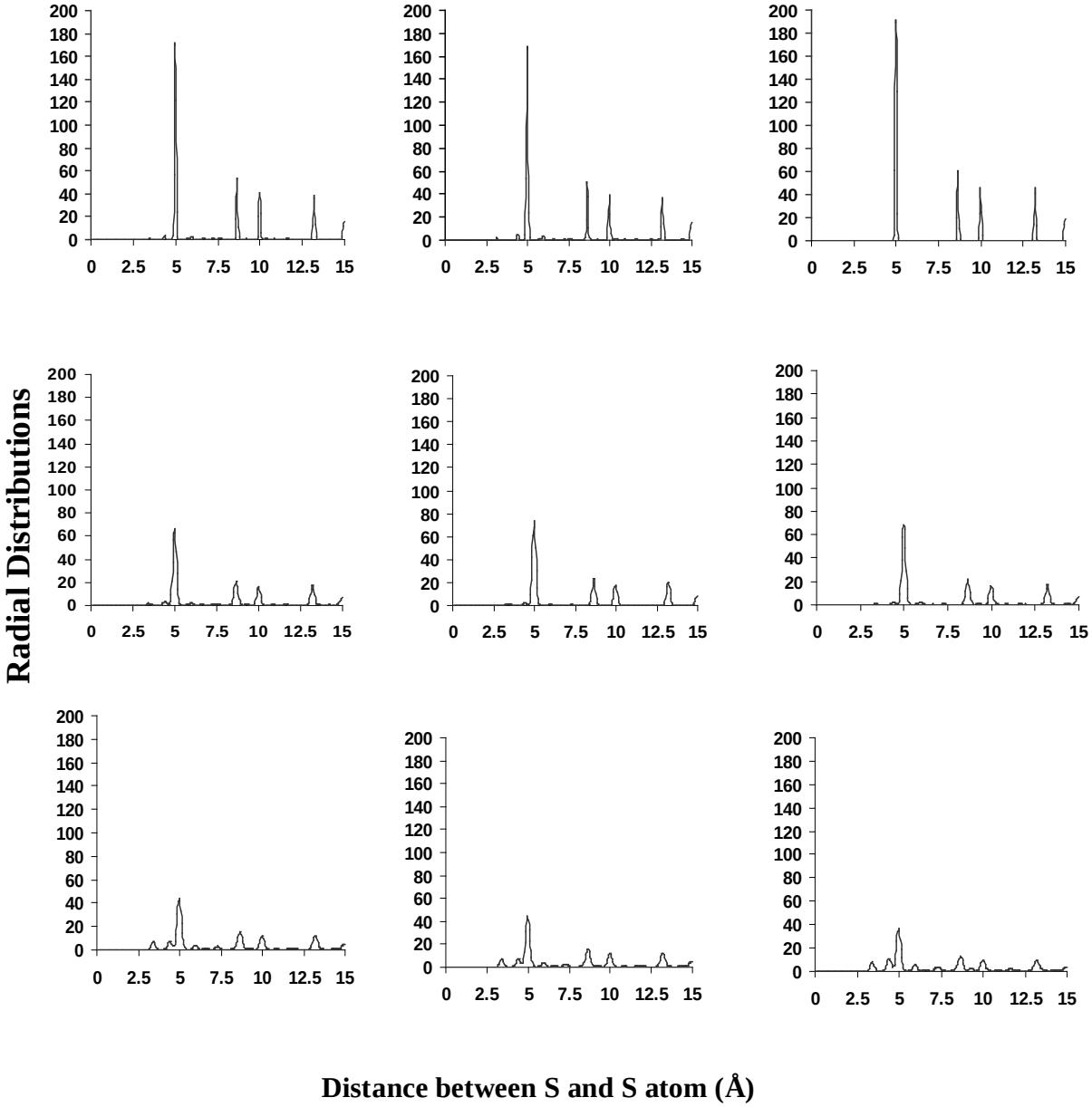

Figure 3-9. Radial Distribution functions. A) Radial distribution functions of S atoms in alkanethiol molecules. From left to right are the *cis*-containing monolayer, the *trans*-containing monolayer and the pure monolayer at (top to bottom) 50 K, 350 K, and 375 K, respectively, B) Snapshots of the positions of the S atoms on the surface at 50 K (top) and 400 K (bottom).

B

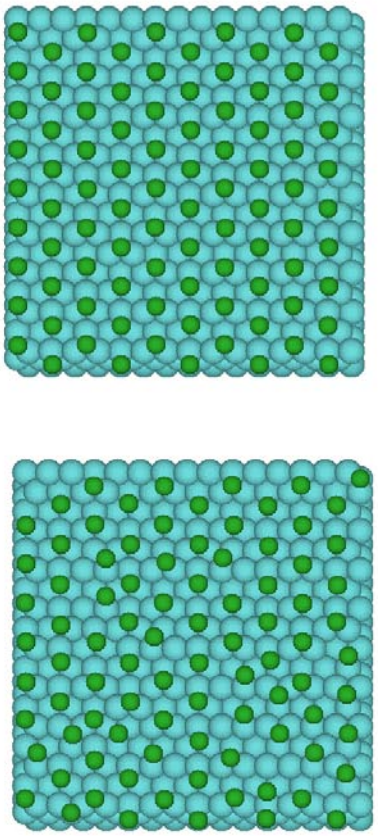

Figure 3-9. Continue

A

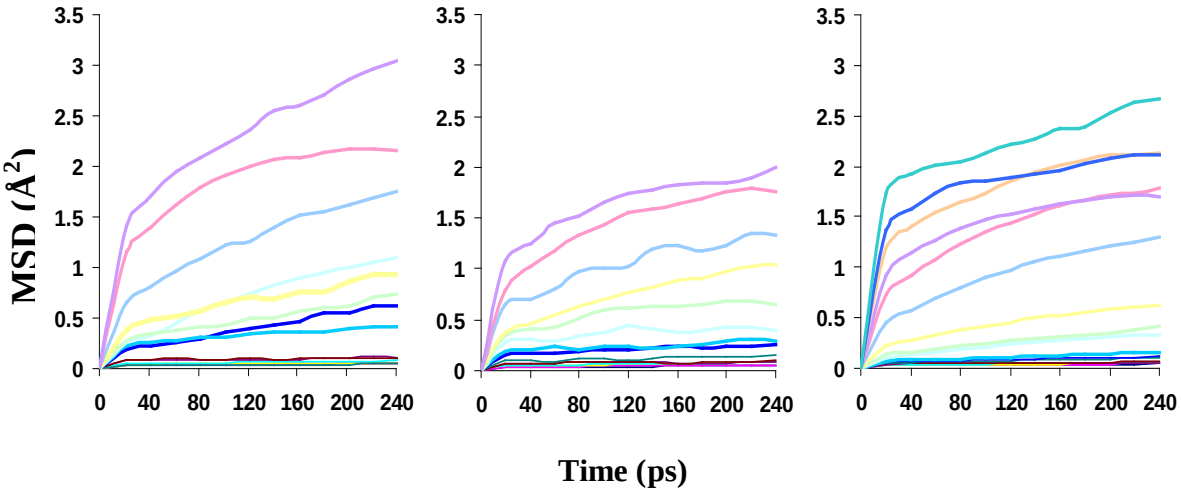

B

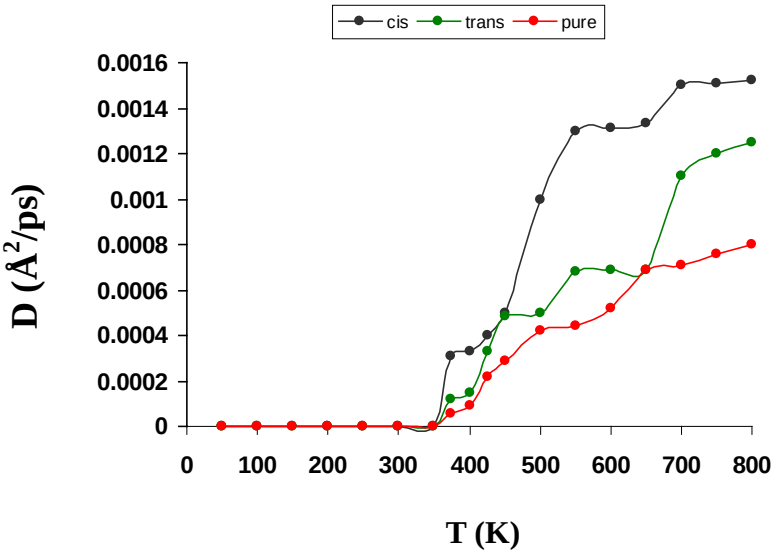

Figure 3-10. Diffusion process. A) Mean square displacement (MSD) of sulfur atoms as a function of temperature (50K to 800K). Left to right are the *cis*-containing monolayer, the *trans*-containing monolayer and the pure monolayer, B) Diffusion coefficient (D) versus temperature (T)

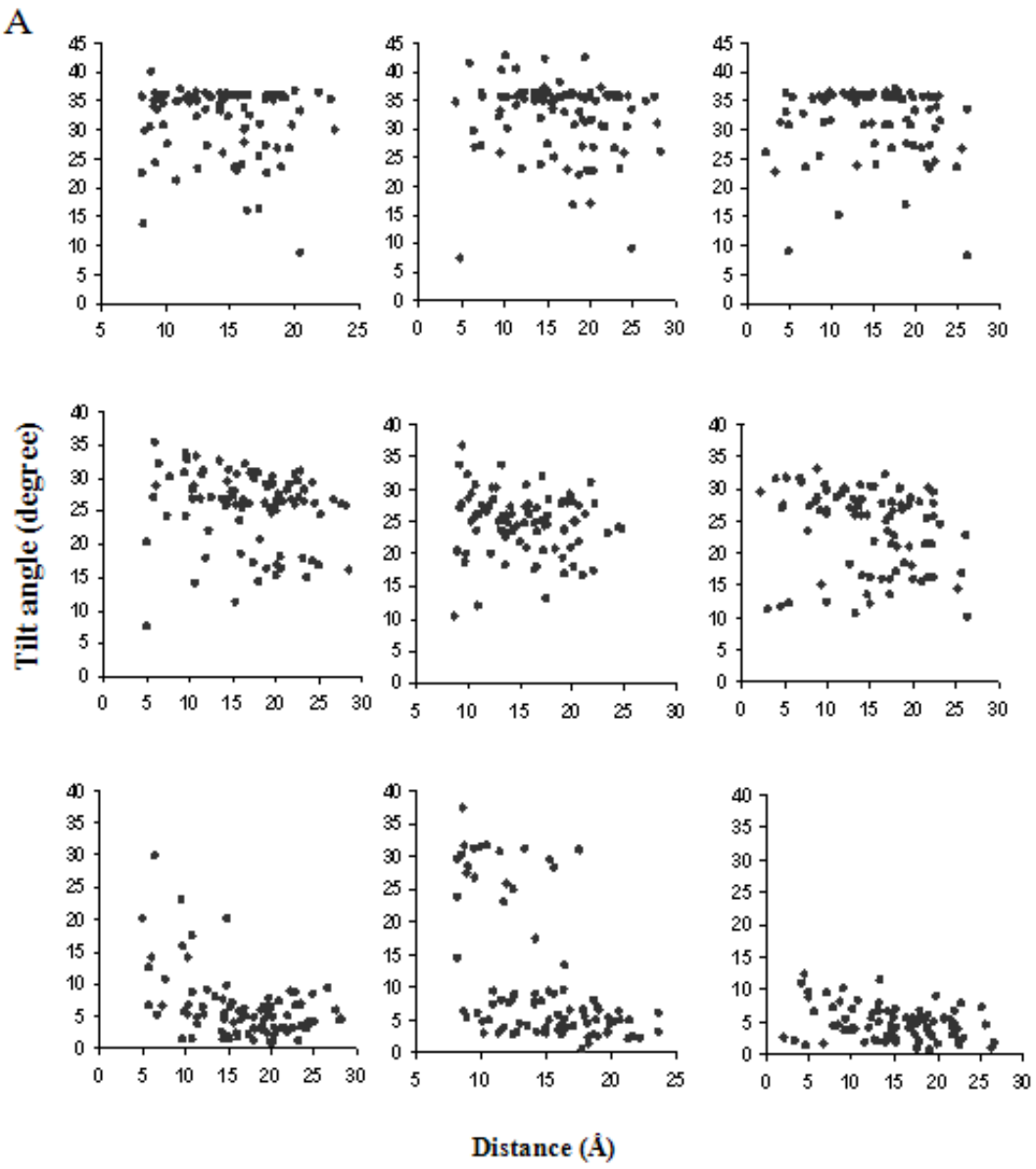

Figure 3-11. Angle Distributions and guest molecule relation. A) Tilt angle of the host alkanethiol molecules as a function of the distance from a guest molecule. From left to right are the *cis*-containing, the *trans*-containing and the pure monolayer, at temperature of 50 K, 350 K, and 375 K, from top to bottom.. The distance is measured between two S atoms attached to the surface. For the pure monolayer, the center alkanethiol molecule serves as the reference, B) Height of the molecules, from the surface to the terminal atom, as a function of distance from a guest molecule. From left to right are the *cis*-containing, the *trans*-containing and the pure monolayer at (top to bottom) 50K, 350K, and 375K, C) Distributions of molecular height during the simulations. From left to right are the *cis*-containing, the *trans*-containing and the pure monolayer at (top to bottom) 50 K, 350 K, and 375 K.

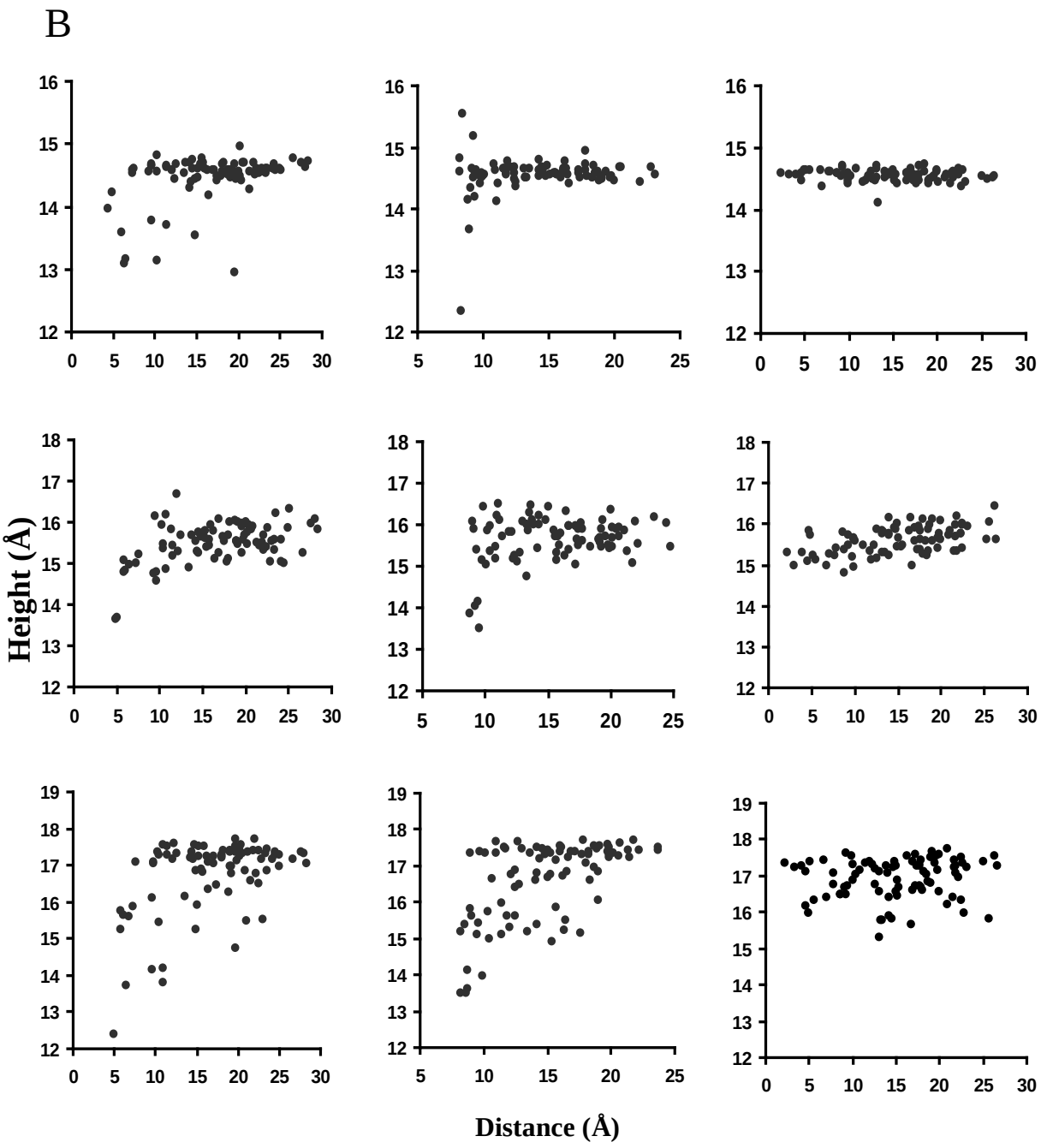

Figure 3-11. Continue

C

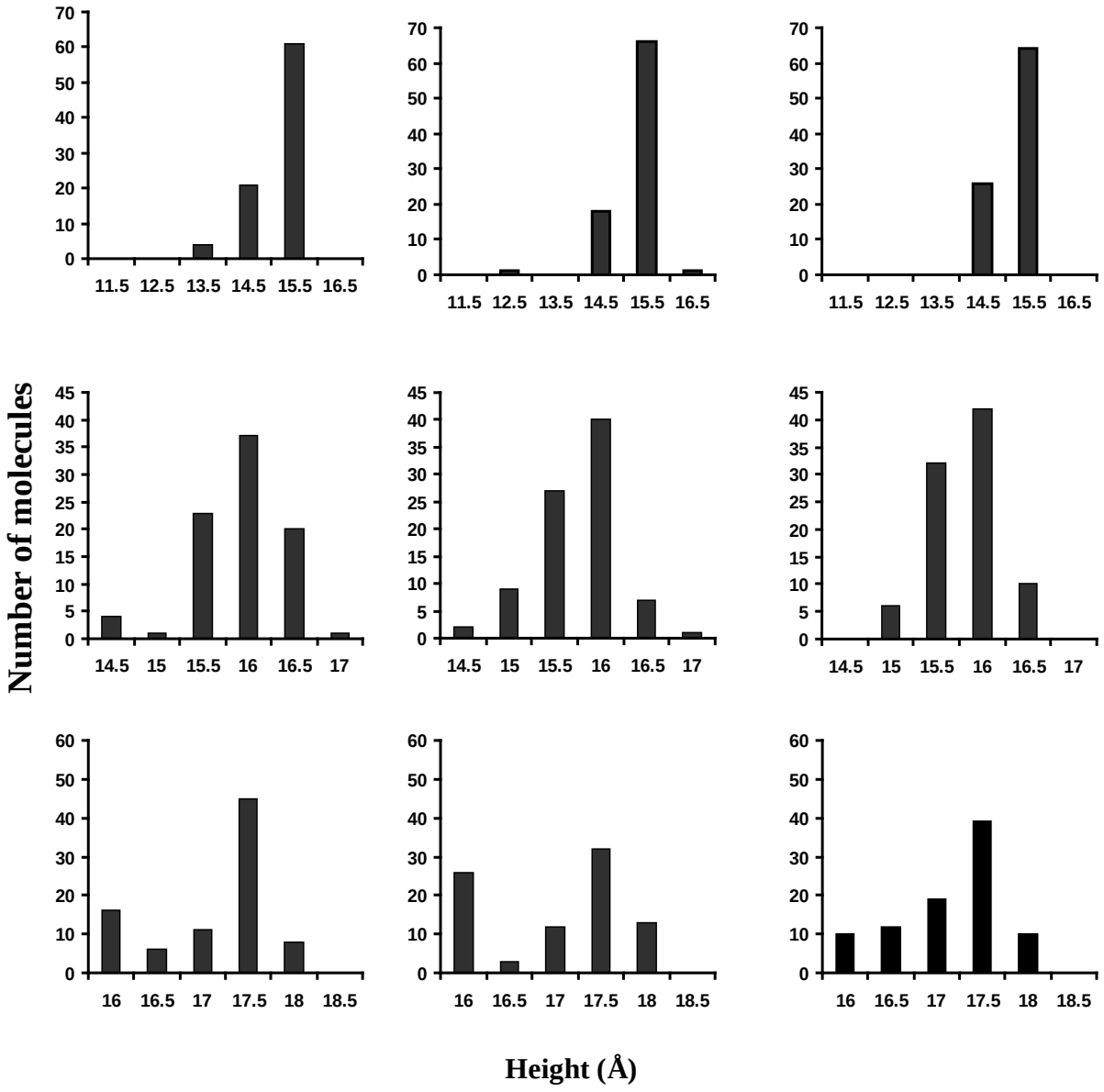

Figure 3-11. Continue

CHAPTER 4
MOLECULAR DYNAMICS SIMULATIONS OF AU PENETRATION THROUGH ALKANETHIOL MONOLAYERS ON THE AU (111) SURFACE

Introduction

Due to their wide range of applications as protective coatings, in surface chemistry, and as bio-sensors,[109, 110] many polymer/organic molecule assemblies have been investigated recently.[2, 81] One prototypical is alkanethiol self-assembled monolayers (SAMs) on the Au(111) surface. This family of molecular assemblies is easy to prepare, structurally simple and has well-defined order. Since their discovery in the early 1980s, these systems have been studied extensively.[1, 87] These systems also serve as test beds for investigations of properties of possible new-generation molecular-electronic devices. The alkanethiol SAM presents a classical metal-insulator-metal (MIM) tunnel junction when fabricated between metal contacts due to their large HOMO-LUMO gap (HOMO: highest occupied molecular orbital; LUMO: lowest unoccupied molecular orbital) of approximately 8 eV.[35-37]

Considerable experimental work has now been performed to investigate the structure and characteristics of alkanethiol monolayers including scanning-tunneling microscopy (STM),[92] low-energy atom diffraction (LEAD),[93] gazing-incidence X-ray diffraction (GIXD)[94] and atomic force microscopy (AFM).[95] These studies have reported detailed structural information about such monolayers including the tilt angles of the alkanethiol chains, temperature effects, and the coverage and the chain length dependence of the properties of the monolayers.

Recent experiments aim at using an Au/SAM/Au layered structure as a molecular junction.[111-114] One way to prepare an Au/SAM/Au structure is using a vapor deposition technique to deposit Au onto alkanethiol SAMs that are formed on the Au(111) surface.[111, 112] One difficulty with this technique is the possibility that the gold atoms can penetrate through the SAMs at room temperature.[112, 115, 116] Scanning tunneling microscope measurements have shown significant

penetration of Au atoms through CH_3 terminated SAMs.[116, 117] Molecular motion at room temperature causes vacancies that Au atoms can use penetrate through the alkanethiol SAMs.[112, 118]

Experimentally, Zhu and co-workers prepared self-assembled alkanethiol monolayers by adsorption of alkanethiolates on the Au(111) surface and then deposited Au atoms on these monolayers.[112] They applied different surface characterization techniques such as time-of-flight secondary ion mass spectrometry (ToF-SIMS)[111, 118, 119] and AFM.[112] By analyzing the ToF- SIMs spectra, they identified three distinct sets of peaks in the spectra, Au^+, $(C_nH_m)^+$ and $AuS(CH_2)_{16}^+$. No $Au(C_nH_m)^+$ peaks were observed, which indicates that the Au ad-atoms do not remain in between the layers, or on top of the layers. Even after large amounts of Au was deposited, no changes in the spectra were observed, indicating that Au atoms penetrate extensively into alkanethiol SAMs and form metallic layers on the Au/S interface.[112]

In addition to mass spectra, conductance probe AFM (CPAFM) indicated the presence of metallic filaments inside SAMs.[112] Using the tip as the conductance probe enabled detection of the presence of such buried filaments. These filaments can form conduction pathways via tunneling from the tip.[112]

Experiments also indicate that it is possible to reduce the mobility of the Au ad-atoms by decreasing the temperature. Reed and co-workers cooled the SAMs to liquid-nitrogen temperature and observed that the Au atoms did not penetrate the SAMs.[111]

Theoretical work based on molecular dynamics simulations (MD) have also done to study the structure, dynamical and thermodynamic properties of alkanethiol SAM on Au surface[41, 42, 120, 121] as well as impurity molecules in the pure SAMs.[45] These calculations focus on the alkanethiol SAMs, in which molecules interact mainly by weak van der Waals forces. To date, there is no

theoretical investigation that studies deposition of metal ad-atoms which is extremely important to fabricating metal-molecule-metal junctions.

Inspired by the experimental results and the need of understanding the motion of ad-atoms, we have investigated the penetration of Au atoms into alkanethiol monolayers using molecular dynamics simulations. In particular, we performed molecular dynamics simulations starting with placing Au atoms on top of alkanthiol SAMs, which has been thoroughly characterized in our previous investigation.[45] Varying numbers of Au atoms (varying concentration) at a number of randomly selected initial configurations have been simulated at room temperature and low temperature (50 K). To describe the monolayer-Au atom interaction properly, we performed quantum-mechanical calculations to calibrate the MD potential parameters. In addition, we have also investigated the electronic structure of the system, and charge transfer between the monolayer and the Au(111) surface.

The rest of the chapter is organized as follows: Section II describes the computational details, section III are results from the simulations, and we discuss and conclude our investigations at the end.

Computational Details

Our model system consists of an alkanethiol (dodecanethiol) monolayer on a Au(111) surface. The gold surface is modeled using a six atomic layers slab. In the lateral direction, each layer of surface contains 18x15=270 atoms; with a size of 44.9 Å x 43.2 Å. 90 alkanethiol molecules have been placed on the surface to simulate 100% coverage. Periodic boundary conditions have been used in all three directions. But a 20 Å vacuum has been inserted between two adjacent slabs in the z-direction (perpendicular to the surface) to model a Au(111) surface. The MD unit box had the shape of a hexagonal $(\sqrt{3}\times\sqrt{3})$R30 lattice in the x- and y- directions.

To describe the intra-molecular interactions, we have applied the Dreiding force field.[99] The Au-S interaction were obtained from Sellers,[8] as in our previous publication.[45] The Universal Force Field (UFF)[44] was used to describe the van der Waals interactions, and the interactions between the Au atoms were modeled with the Sutton-Chen potential.[47, 101]

Most of our MD simulations were preformed at 300 K, with a few test cases at 50 K. The Berendsen thermostat[51] has been used for temperature control. Systems that consist gold substrates and alkanethiol monolayers in our studies have been equilibrated (400 ps) before adding extra Au atoms. Typically, we let MD simulation runs go on for about 1.0 ns before collecting final statistical information. Various initial configurations of Au ad-atoms on top of the alkanethiol SAMs have been used to test the sensitivity of the results to the initial conditions and to improve statistics.

To improve the reliability of our MD simulations, quantum-mechanical calculations based density functional theory (DFT)[57] have been performed. The purpose of these DFT calculations is to investigate the binding energy of Au on alkanethiol SAMs, which is critical to the quality of the force-field used for MD simulations, and to analyze the electronic structure of the molecule-metal interface. The DFT calculations have been performed using the (VASP)[58, 59] program with the projector augmented wave method (PAW)[60] and generalized gradient approximation (GGA); specifically the PW91[61] exchange functional. For quantum modeling, we have used a slab of 5 atomic layers for surface calculations. A vacuum of thickness of 15 Å between two neighboring slabs have been inserted in the z-direction. An energy-cutoff of 300 eV, a 4x4x1 k-point Monkhorst-Pack[62] mesh, and a Methfessel-Paxton smearing[63] of 0.2 eV, have been used. The systems have been relaxed until the force on each atom is below 0.02 ev/A.

Results

Binding Energy of Au on Alkanethiol SAMs

As a fist step we have tested the UFF to determine whether or not this potential is adequate to describe the interactions of the Au ad-atoms with the alkanethiol SAM. We have found that the classical UFF force field gives a binding energy of -0.7 kcal/mole between an ad-atom and the alkanethiol-Au(111) surface. In contrast, the DFT calculations give a binding energy of -7.0 kcal/mole, which is a factor of ten greater in magnitude. This difference suggests that modifications of empirical potential are necessary.

Our first test of the UFF has involved calculations of the Au-alkanethiol potential as a function of the distance of the Au atom above the surface. Figure 4-1 shows configurations of a system composed of four alkanethiol molecules per unit cell connected to a slab of 60 Au atoms (5 layers, 12 atoms in each layer with the bottom two layers fixed). One Au ad-atom has been placed at various heights within the monolayer. The optimizations have been performed with the z-coordinate constrained, except for the initial and final configurations, in which full relaxation has been allowed. Note that the constraint does not apply to the x and the y directions. Similar calculations have been performed for two systems. In the first one (Figure 4-1), the alkanethiol species are tilted by 35^0, and in the second, the alkanethiols are vertical (Figure 4-2), corresponding to low temperature and high temperature, respectively.[45] In the z-direction, the ad-Au atom was constrained in positions ranging from 18 Å to 3Å above the slab. When the z-component was allowed to relax, the ad-atom penetrated the monolayer to the top of the Au/S interface.

Figure 4-3 shows the binding energy of the Au ad-atom as a function of z. Fig. 4-3a shows the results of the DFT calculations, and Fig. 4-3b shows the results with the Au-monolayer potential scaled by a factor of 10. Clearly, the agreement between the DFT results is much better

with the scaled UFF parameters. This provides the rationale for scaling the UFF parameters in the dynamics calculations, as described below.

In addition to this, we calculated the binding energy of the vertical and the tilted alkanethiol molecules on the Au(111) surface. Binding energy of one vertical alkanethiol turned out to be -34.1 kcal/mol and the binding energy of one tilted alkanethiol is -29.9 kcal/mol.

Molecular Dynamics

To examine the extent to which gold ad-atoms penetrate the alkanethiol SAMs, and how this penetration depends on surface coverage and temperature, we performed detailed molecular dynamics simulations of the entire ad-atom plus SAM plus gold slab system.

Our first tests used the unmodified UFF parameters to describe the interaction between the Au ad-atoms and the monolayer. We found that with this force field we could not reproduce event the qualitative aspects of the experimental results. Rather than interacting with the SAM, the gold atoms simply flew away. Based on our comparisons of the potentials with DFT (see Fig. 4-3), we repeated the calculations with the relevant UFF potential parameters scaled by factors of 5 and 10. To do this, we simply scaled the potential well-depth values (e in the formula) in the UFF. The potential has the form $U(r) = 4*e*[(\sigma/r)^{12} - (\sigma/r)^{6}]$ and here we scaled only the Au-C and Au-H interactions and did not modify the Au-S parameters. Only Au ad-atom and molecule interaction has been scaled.

In the first set of simulations, 9 gold atoms were placed Au at random configurations on top of alkanethiol SAMs (i.e. 9 Au atoms/90 molecule). The simulations were run with the UFF parameters scaled by a factor of 5. The results showed that most of the Au atoms were clustered on top of the monolayer. Some atoms left the surface and a small number penetrated the monolayer (see Fig. 4). Next, we scaled the UFF parameters by a factor of 10 and repeated the simulations. In this case, the results showed that most Au atoms penetrate the monolayer (see Fig. 5). Histograms

of the z-values of the gold ad-atoms (averaged over five different initial conditions are show in Fig. 4-6a, in which the potential is scaled by a factor of 10, and Fig. 4-6b, in which the potential is scaled by a factor of 5. In the histograms the top-most gold layer has a z-value of -3 Å and the bottom layer has a z-value of -15 Å. The peak at -15 Å is an artifact due to periodic boundary conditions (atoms leave the surface and they appear at the bottom layer). Figure 4-6a shows large peaks near 0 Å, which indicates that most of the atoms penetrate the alkanethiol monolayers and form films at the Au/S interface. In figure 4-6b, in contrast, most of the Au ad-atoms cluster on top of alkanethiol monolayers, as show by the peaks near 15-20 Å. Note that that the results in Fig. 4-6a, which are consistent with those seen in the experiments, are also consistent with the predictions of the DFT calculations (see Fig. 4-3)

To test the effects of initial coverage, we repeated the simulations with 18 Au ad-atoms on the alkanethiol SAMs. The same procedures were followed and similar results were obtained. The histograms of the average z-values of the Au ad-atoms can be seen in Fig. 4-7. As in Fig. 4-6, when the UFF parameters are scaled by a factor of 5, clustering occurs on top of monolayers, resulting in peaks near 15 and 20 Å. When the parameters are scaled by a factor of 10, the Au ad-atoms penetrate into the alkanethiol molecules and form buried layers on the Au/S interface, as evidenced by the large peak at 0 Å. As seen in the experiment,[112] the main result of increasing the initial coverage is to create additional buried layers.

Density of States and Charge Transfer

The molecular dynamics simulations, in agreement with experiment, provide strong evidence that Au ad-atoms have a high propensity to penetrate the alkanethiol monolayer and interact strongly with the surface. To investigate the nature of this interaction, we have performed density of states (DOS) and projected DOS (PDOS) calculation to examine the changes in electronic structure, and to analyze the mechanism of charge transfer within the system. The DOS and PDOS

of the two systems, one without and one with a gold ad-atom, are shown in Fig. 4-8, and Fig. 4-9, respectively, and the DOS and PDOS of the pure Au surface are shown in Fig. 4-10 for comparison. The figures show that while d-orbitals dominate the DOS below -1 eV (measured from E_F) in pure Au surface, s-, p- and d-orbitals have approximately equal contributions to the DOS near E_F (-1 to 1 eV). The tilted and vertical molecule systems produce very similar DOS and PDOS, meaning that the tilting angle of the thiol molecule has little influence on the electronic structure of the surface. From Fig. 4-8 and 4-9, we also see that a single ad-atom modifies the DOS/PDOS only moderately, the Fermi level is shifted by ~0.25 eV in both the tilted and vertical cases. In both systems with and without ad-atom, the PDOS on the Au surface is almost identical to that for the pure Au surface. However, a more careful separation of PDOS (Fig. 4-11) shows that the electronic structure for the topmost layer of Au surface actually changes drastically, especially around 2.0 eV to 3.0 eV below E_F; while other layers that is not directly bonded with the molecules are not substantially affected. This clearly shows the screening effect of a metallic substrate, and thus the modification is limited very close to the surface.

To analyze the nature of the charge transfer, the PDOS is integrated of various regions of the system. The DOS data shows that the charge transfer to both tilted and vertical molecules from the gold surface is ~1.4 electron.

Table 4-1. Charge transfer (per molecule) from the Au surface and charge transfer to alkanethiol molecules

System	Δ_1(e)	Δ_2(e)
Vertical molecule on the surface	-0.36	+0.36
Tilt molecule on the surface	-0.35	+0.35
Vertical molecule and the Au ad-atom on the surface	-0.12	+0.41
Tilt molecule and the Au ad-atom on the surface	-0.13	+0.39

Δ_1 charge transfer from the Au surface
Δ_2 charge transfer to the alkanethiol molecules

Once an ad-atom is attached to the surface, the Au ad-atom transfers ~1.1 electrons to the molecule, which reduces the charge transfer from the Au surface to ~0.5 electrons. The PDOS analysis, which shows that the ad-atom induces a shift of the Fermi level, agrees with the charge-transfer data. The data also show that the detailed structure (tilted or vertical) does not alter the charge transfer substantially, which is also consistent with the PDOS analysis.

Conclusions

In this chapter, we analyzed the penetration of Au ad-atoms through alkanethiol SAMS using computational methods. Quantum mechanical calculations were performed to modify the classical potential parameters. When the potentials were changed to match the experimental interaction energies, we found that the ad-atoms penetrate the SAM readily and form buried layers at the Au/S interface. The coverage and temperature dependence observed in the simulations are in good agreement with the experimental results. In particular, we found that, there is extensive penetration of Au atoms in the molecules at 300 K. At 50 K, there is no Au penetration inside the monolayer during simulations (trajectories are 20 times as long as the cases of 300 K, i.e. 20 ns). When the Au coverage was increased, the Au ad-atoms continued to penetrate the monolayer and formed buried layers beneath the SAM. To match the experimental results, the UFF interactions between the Au ad-atoms and the monolayer were scaled by a factor of ten. These results are a warning to the community that "universal" force fields may require modifications in systems outside of the range in which they were calibrated. Calculations of the DOS and PDOS revealed detailed information about the electronic structure and charge transfer between the alkanethiol monolayer and the Au(111) surface. We expect that these results will be important for the design of new generation molecular-electronic devices. We believe our calculations will inspire new research in constructing new Au/SAM/Au sandwich structures. For the specific system investigated in this work, for example, it is clear that producing layered structures using the methods suggested

experimentally will require passivating the SAM in some way to prevent penetration by the Au ad-atoms.

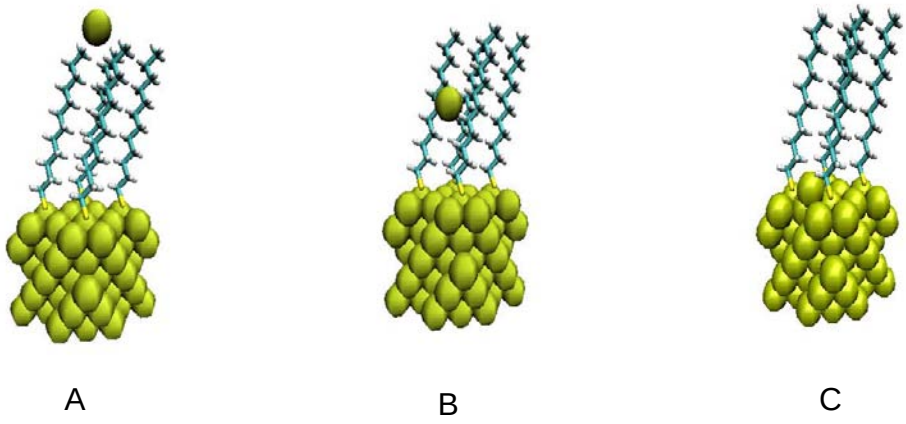

Figure 4-1. Snaphots of a system with four tilted alkanethiol molecules attached to a model of the Au(111) surface with an Au ad-atom after relaxation with DFT. A) 18 Å above the surface, B) 9 Å above the surface and C) interacting with the Au/S interface.

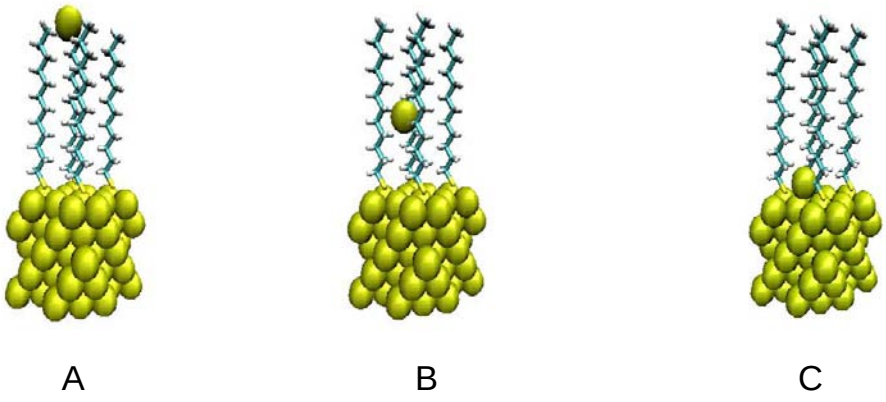

Figure 4-2. Snaphots of a system with four vertical alkanethiol molecules attached to a model of the Au(111) surface with an Au ad-atom after relaxation with DFT. A)18 Å above the surface, B) 9 Å above the surface and C) interacting with the Au/S interface.

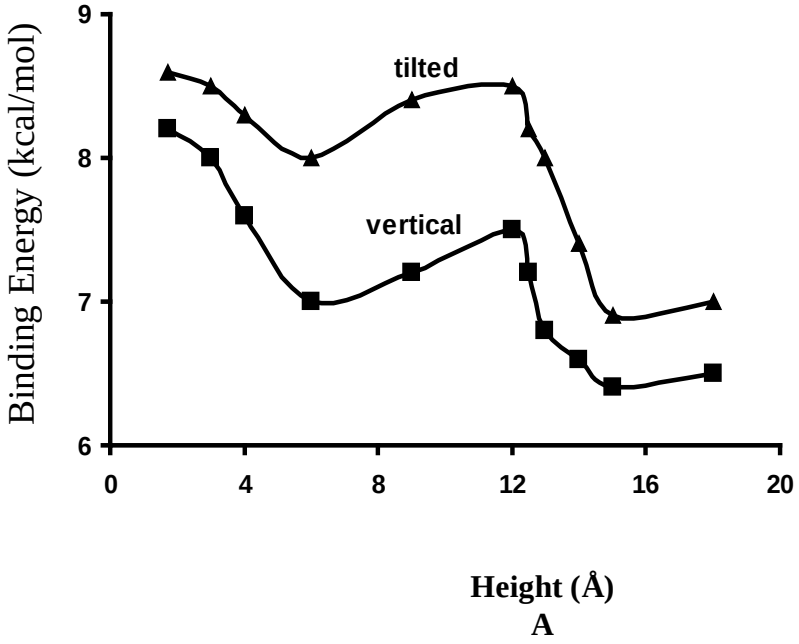

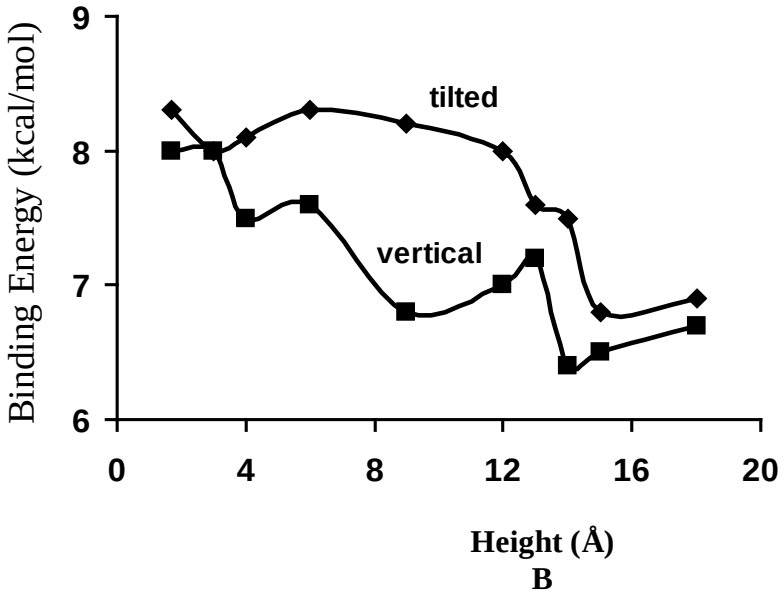

Figure 4-3. Binding energy of the Au ad-atom with respect to the distance above the the Au/S interface. A) DFT and B) the modified UFF as described in the text. Results are presented for both the tilted monolayer and the vertical monolayer.

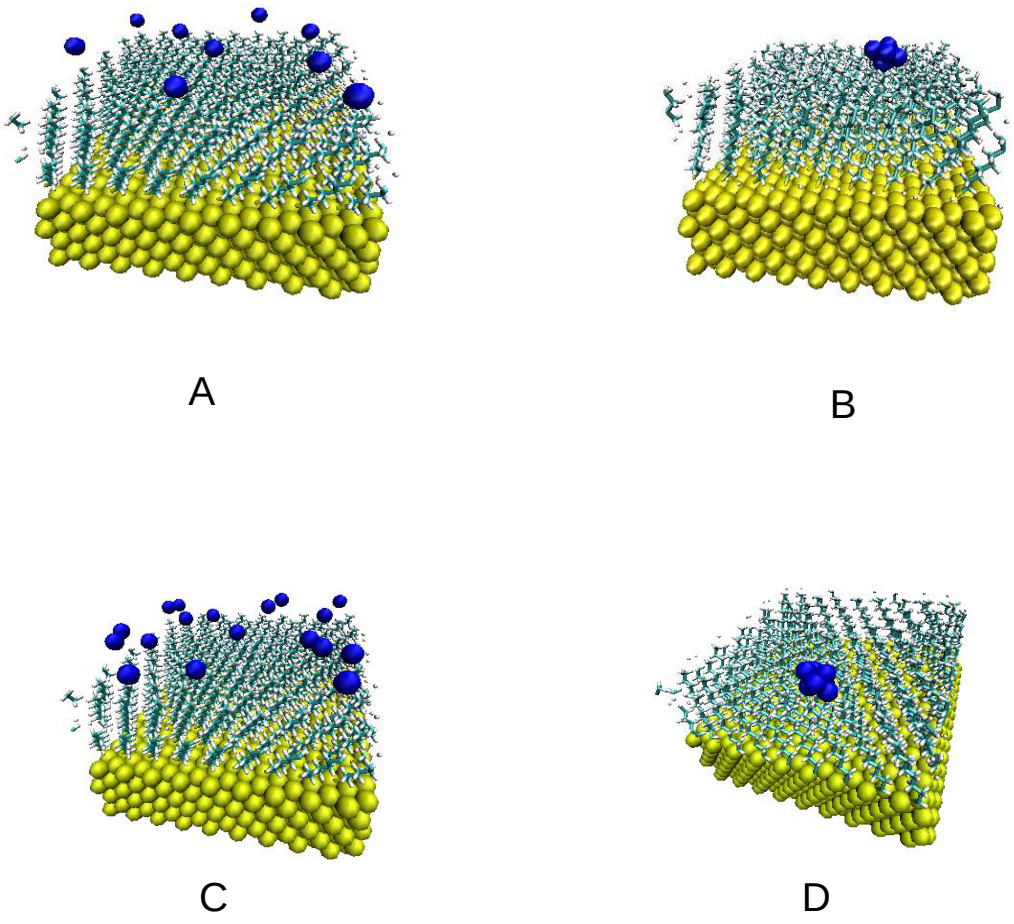

Figure 4-4. Snapshots from the molecular dynamics simulations for 9 atoms placed on the alkanethiol SAMs. A) initial configuration, B) snapshot after 1ns of simulation with the UFF parameters scaled by a factor of 5, C) initial configuration for 18 Au atoms placed on the alkanthiol SAMs, D) snapshot after 1ns simulation, UFF parameters are scaled by a factor of 5.

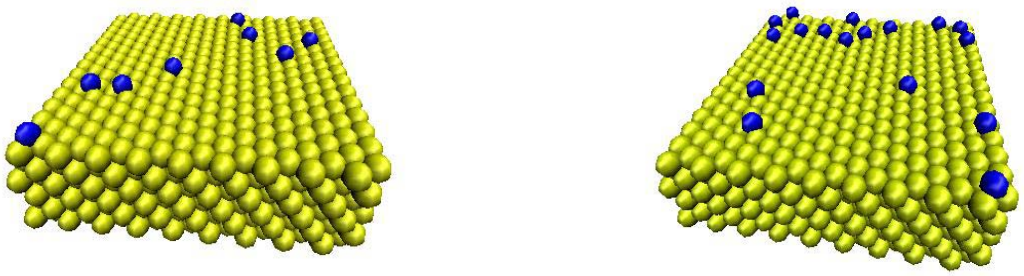

A B

Figure 4-5. Snapshots from the molecular dynamics simulations for 9 atoms placed on the alkanethiol SAMs. A) initial configuration, B) snapshot after 1ns of simulation with the UFF parameters scaled by a factor of 10, C) initial configuration for 18 Au atoms placed on the alkanthiol SAMs, D) snapshot after 1ns simulation, UFF parameters are scaled by a factor of 10.

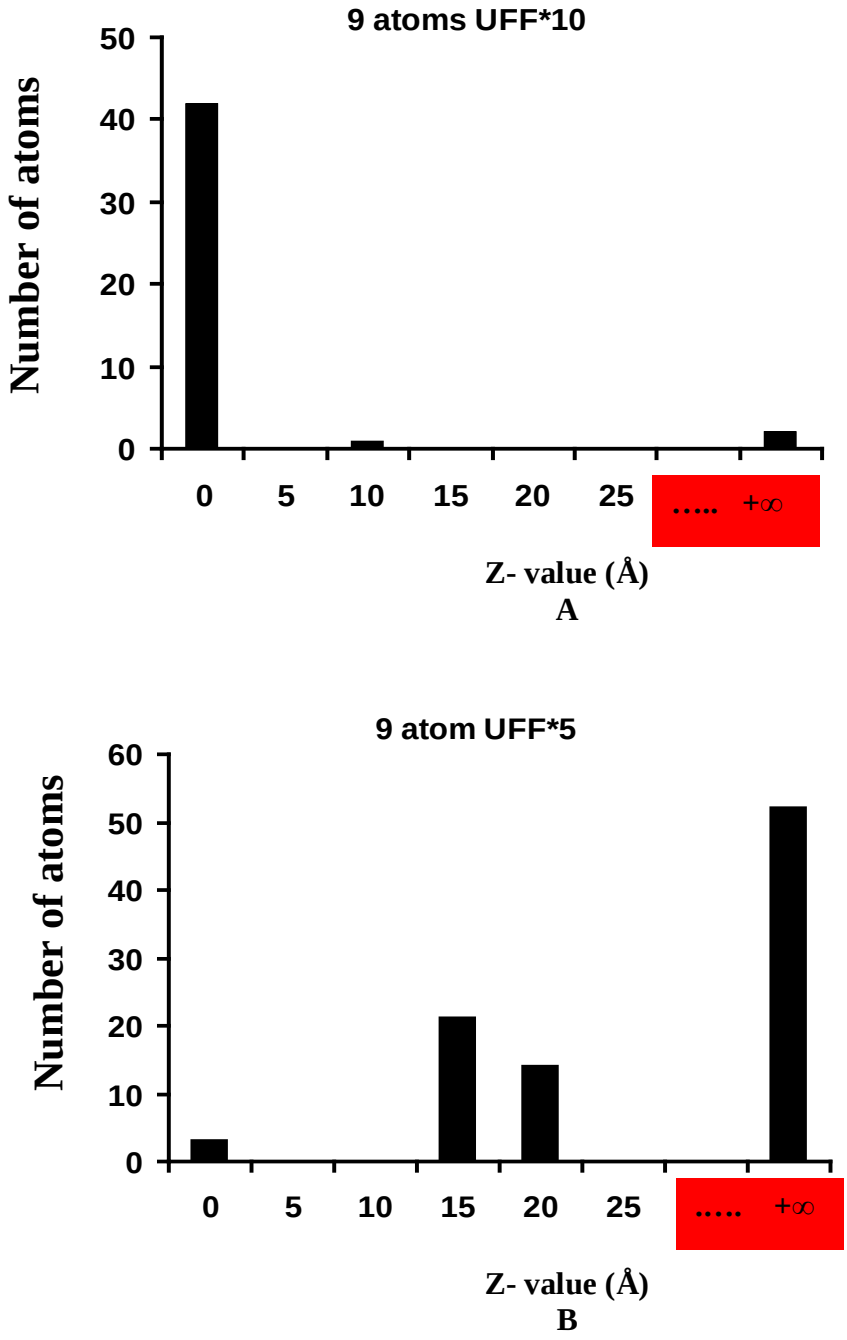

Figure 4-6. Average histograms of z, the distance of the Au ad-atom above the surface, for 9 atoms on the SAMs. A) the UFF scaled by a factor of 10 and B) the UFF scaled by a factor of 5.

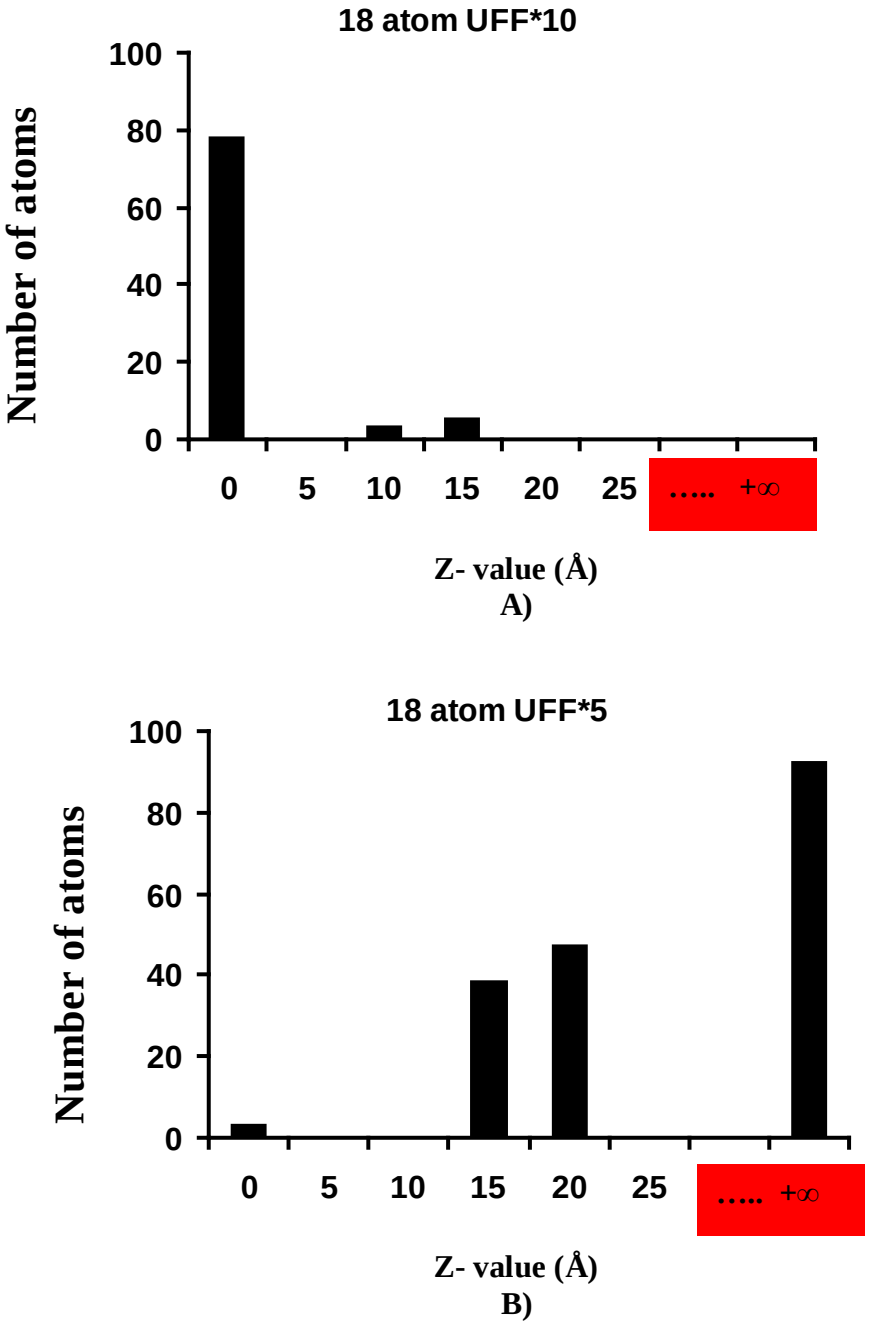

Figure 4-7. Average histograms of z, the distance of the Au ad-atom above the surface, for 18 atoms on the SAMs. A) the UFF scaled by 10 and B) the UFF scaled by 5.

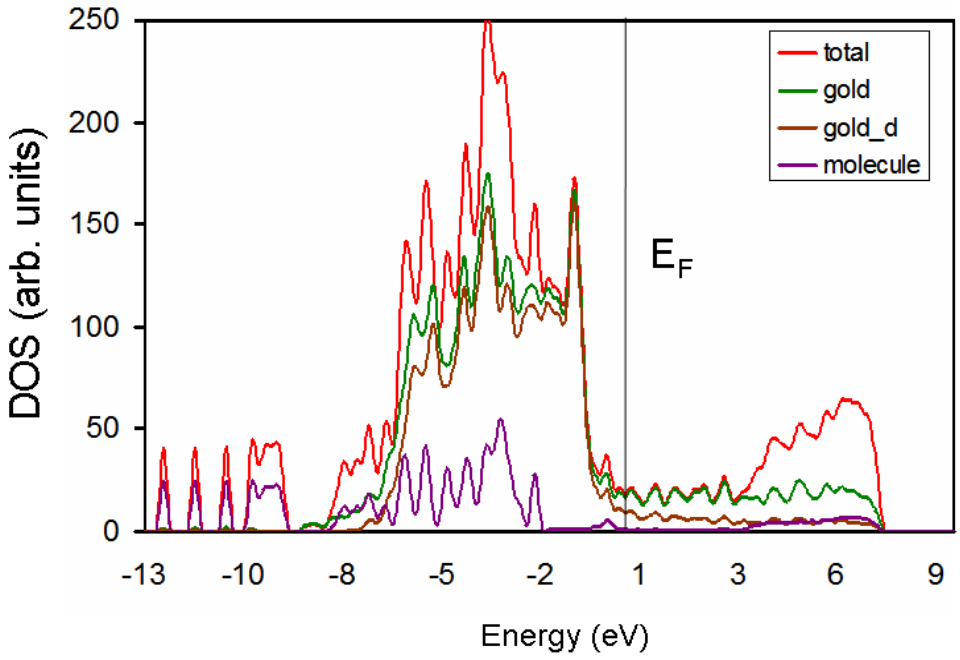

A

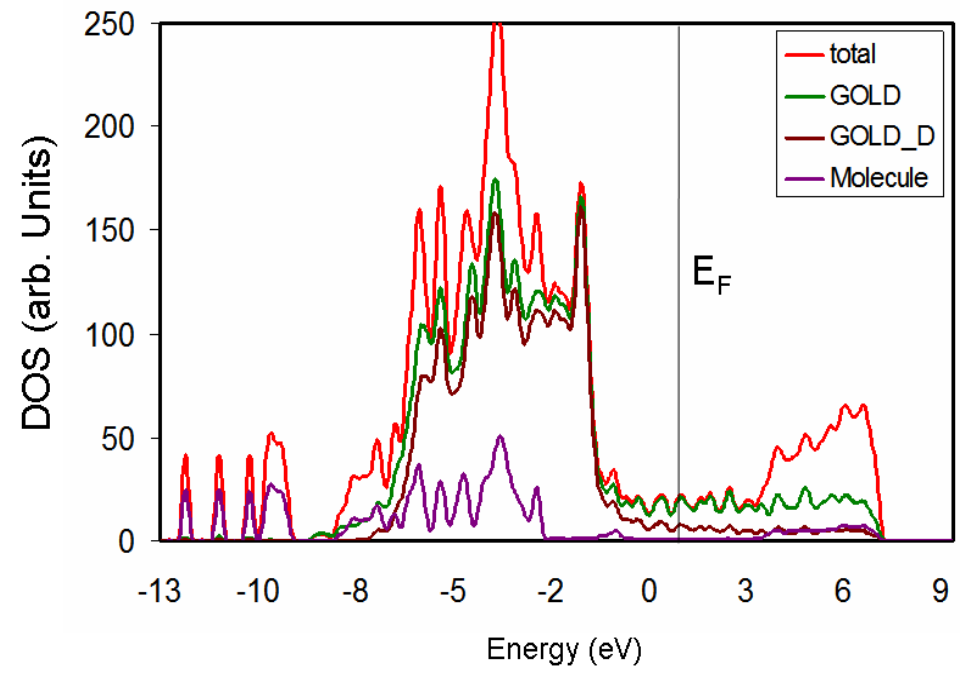

B

Figure 4-8. DOS and PDOS for the system without the Au ad-atom. A) Vertical molecules on Au surface, total DOS, projected DOS on Au, projected DOS on Au d- orbital and the total DOS on molecules, B) Tilted molecules on Au surface, total DOS, projected DOS on Au, projected DOS on Au d- orbital and the total DOS on molecules.

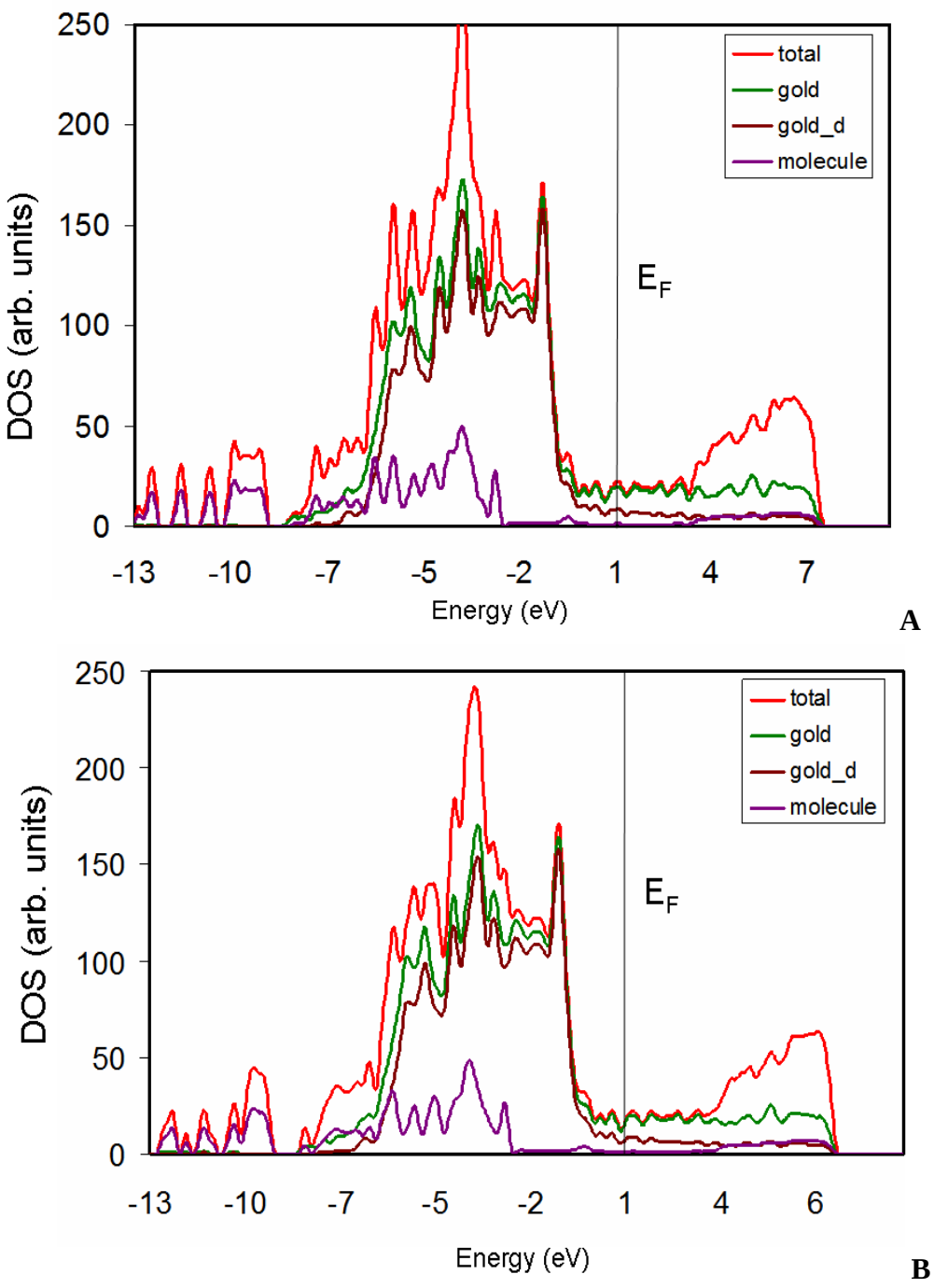

Figure 4-9. DOS and PDOS of the system with the Au ad-atom. A) Vertical molecules and the Au ad-atom on Au surface, total DOS, projected DOS on Au, projected DOS on Au d-orbital and the total DOS on molecules, B) Tilted molecules and the Au ad-atom on Au surface, total DOS, projected DOS on Au, projected DOS on Au d- orbital and the total DOS on molecules.

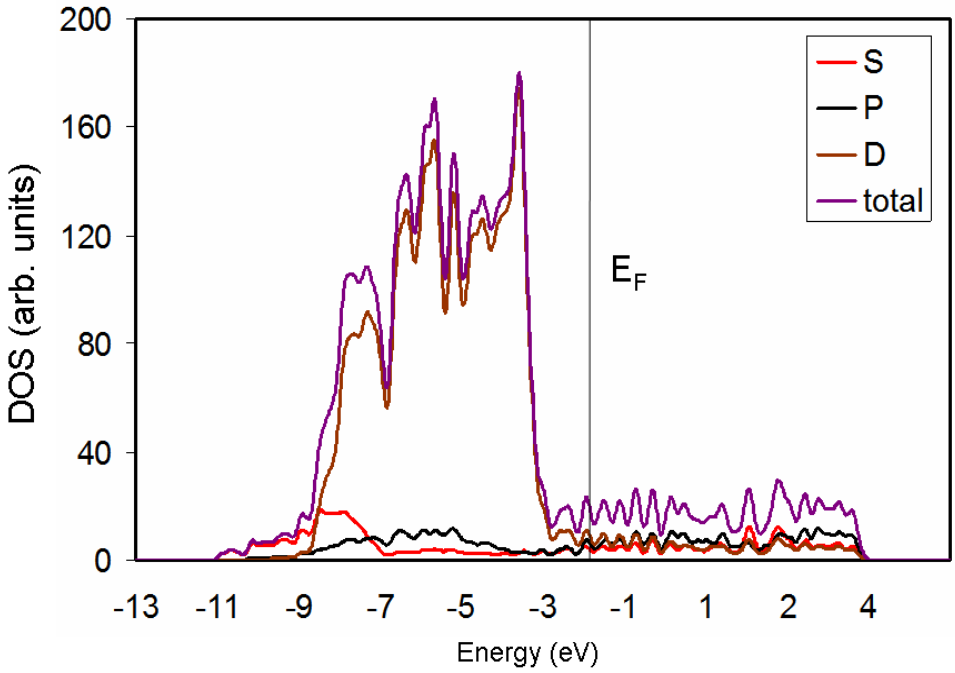

Figure 4-10. Pure Au surface, S, P and D projected DOS and the total DOS.

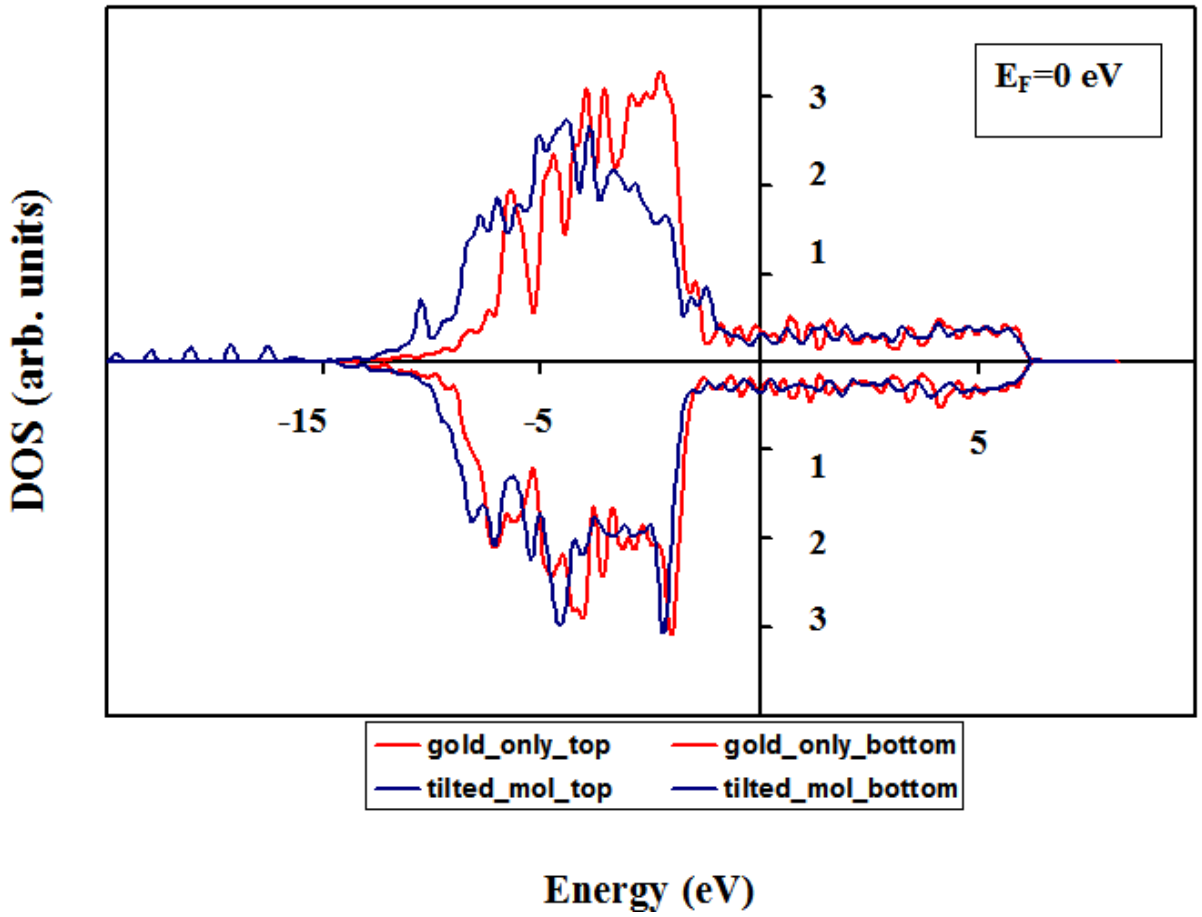

Figure 4-11. Renormalized PDOS for the topmost layer in the upper panel and the rest of the surface in the lower panel.

CHAPTER 5
DYNAMICS OF SILVER CLUSTERS ON ALKANETHIOL MONOLAYERS ON AU(111) SURFACE

Introduction

Intense investigation of metal-organic interfaces over the past decade has revealed a vast range of applications in nano-molecular electronics[80, 122-124] and as electrochemical and optical bio-sensors.[109, 125-128]Diffusion of nano-particles at such interfaces is of fundamental importance in the making of functional nano-structures. Unlike diffusion in solid surfaces, which has been studied,[129-131] the motion of particles on organic molecular surfaces has yet to be explored and offers new possibilities for observing complex phenomena.

Metal clusters, especially metals Au and Ag are the most popular candidates for constructing two-dimensional quantum dot arrays.[132-136] Small metal clusters have interesting spectroscopic properties that are different from those of their bulk counterparts and they can also be used to immobilize large molecules such as proteins.[137, 138] A great expectation is emerging that one can utilize special features of nano-structured matter in future technology. Growing nano-size clusters on surfaces can be traced back to the early 1990s. There have been two basic experimental techniques, one that involves size-selected clusters pre-formed in a chamber and beamed down at the surfaces; and a second that employs self-assembly methods in which clusters form on the surface.[132, 139] Theoretical investigations in the early- to mid- 1990s attempted to understand the control mechanisms of the deposition process.[140, 141] Since the mid 1990s, studies of nano-structured entities have attracted immense attention and much effort has been made to create structures with characteristic sizes in the range 1-100 nm.

One motivation for investigating metal clusters on organic surfaces is to control the interface of metal-organic-metal junctions. In contrast to generating nano-dot arrays, the idea is to force metal atoms to coalesce in a controlled way. Because of the strong cohesive energy between

metal and inorganic materials (silicon etc.), metal clusters on surfaces must be passivated by organic molecules or separated by an inactive matrix. For gold and silver clusters, molecules with thiol groups are often used to passivate the cluster surfaces.[133-135] A natural alternative is to passivate the bulk surface instead of clusters. Self-assembled monolayers (SAMs) of alkanethiol on Au(111) surfaces are particulary widely used in surface studies because they are structurally simple, thermodynamically stable, and have well-defined order.[45, 84, 142, 143] Previous studies found that atomic diffusion through organic layers prevents the formation of a quality junction.[144]

Controlled deposition or growth of unpassivated metal clusters over organic surfaces would provide a novel way of creating nano-particle arrays or growth of metal-organic-metal junctions. For this purpose, understanding diffusion of atoms and nano-clusters on organic assemblies is of essential importance. We therefore choose this system for study.

In a recent paper, we presented an extensive investigation of the dynamics and thermodynamics of alkanethiol monolayers[45] and the properties of such monolayers in the presence of guest molecules. In this work, using a similar molecular dynamics simulation method, we focus on the dynamics of silver clusters Ag_n, with n=55, 147 and 1289, deposited on alkanethiol monolayers self-assembled on Au(111) surfaces. Clusters with 55 and 147 atoms, known as magic number clusters, are complete-shell Mackay icosahedra and have high stability. For the 1289 atom cluster, structure relaxation leads to the formation of facets and the loss of high symmetry, but the detailed structure of the cluster is not an important factor in the physics we present in this chapter.

Computational Details

Metal-metal interactions follow the Sutton-Chen[47] potential, the non-bonding VDW interactions are described with the Universal Force Field (UFF),[44] and the Au-S interaction are of a LJ form obtained from the previous work of Sellers,[8] as also in our previous work.[45] The intra-

molecular interactions for the alkanethiol molecules are described with the Dreiding force field.[99] The MD unit box has the shape of a hexagonal $\left(\sqrt{3}x\sqrt{3}\right)R30^o$ lattice in the x- and y- directions. In the lateral direction each layer consisted of 18x15=270 atoms, with a size of 44.91 Å by 43.2 Å. The gold atoms were held fixed during the simulations. Ninety alkanethiol molecules were placed on the surface, for 100 % coverage. Periodic boundary conditions were used in all three directions. A 20 Å vacuum was inserted between two adjacent slabs in the z- direction to model the (111) surface. To follow the diffusion of bigger clusters (147, 1289 atom) we used a surface four times larger.

The clusters (n=55, 147, 1289) were placed on dodecanethiol SAMs (the closest distance between Ag and alkanethiol atoms was about 3 Å). The systems were relaxed at 0K during a 10ns (4ns equilibration time) simulation. The binding energies of these clusters were -4.7 kcal/mole for the smallest one, -5 kcal/mole for the mid-size one and -14 kcal/mole for the largest cluster. After the relaxation, simulations were performed at 150K to investigate the diffusion and sintering; the NVT Brendsen[51] thermostat was used to maintain a constant temperature. This temperature was chosen because at higher temperatures all but the largest cluster are unbound and fly away from the surface. For the smallest cluster we obtained 130ns of simulation time (in all simulations the first 10ns simulation contains 4 ns of equilibration time). For the mid- size cluster the total simulation time was 80 ns, and for the largest cluster, the total simulation time was 70 ns. As an additional test, we placed four 55 atom clusters on a surface a factor of four larger and ran simulations at 150K. In this case, the four clusters eventually collided with one another and formed one large cluster. Figure 5-1 shows a snapshot of a typical simulation configuration, including the gold substrate, the alkanethiol SAM, and a 55 atom cluster.

Results

Figure 5-2 shows the *x*-*y* surface projection of the trajectory of the cluster center of mass for three clusters. The 55-atom cluster trajectory, which lasts 130ns, is composed of three separate segments, between which the cluster briefly leaves the surface. The 147-atom cluster trajectory covers 80ns, and the 1289-atom cluster trajectory lasts 70ns. The trajectories display, in a general sense, a wandering "random walk", but the nature and the scale of the wandering is very different from the smallest to the largest cluster, differences that we quantify in the following analysis.

All components of velocity are Gaussian distributed to high accuracy for all three clusters, with *2-d x-y* variance consistent with the expected $\left\langle \Delta \upsilon^2 \right\rangle = kT/m$. Measured variances are slightly anisotropic, broader in one direction and narrower in another. The anisotropy is greatest for n=1289, where the excess is ±2.3%, only a 2.1-σ effect. However, the velocity correlations are very different for different size clusters. Figure 5-3 shows the spectral densities of *x*- and *y*-components of the velocity, normalized by the velocity variance. The spectrum of the 55-atom cluster spectrum is almost scale free, similar to the characteristic behavior of Brownian motion, for which, as an integral of uncorrelated kicks, the velocity has an f^{-2} spectrum. The spectrum of the 147-atom cluster shows hints of a characteristic scale. The 1289-atom cluster has distinct peaks that are at different frequencies for *x*- and *y*- components. Inserts show the correlation function $c(t)$ of the vector velocity, $c(|t_1 - t_2|) = \left[\langle \upsilon(t_1) . \upsilon(t_2) \rangle - \langle \upsilon_1 \rangle . \langle \upsilon_2 \rangle\right] / \Delta\upsilon_1 \Delta\upsilon_2$. All correlations drop sharply, with a time constant of order 0.1 ns or smaller. For the 55-atom cluster the correlation falls off roughly as the exponential of a fractional power, $\exp\left[-(t/\tau)^{\alpha}\right]$, with $\alpha = 0.67 \pm 0.15$ and $\tau = 0.047$ ns. The correlations of the 147- and 1289-atom clusters also show oscillations at multiple frequencies.

Figure 5-4 shows the rms displacement $\left\langle \Delta R^2(t) \right\rangle^{1/2}$ for two points on a trajectory separated by time difference t, averaged over a trajectory. At small times, the motions of clusters of all sizes are nearly ballistic, $\Delta R = \upsilon t$, with $\left\langle \Delta \upsilon^2 \right\rangle = kT/m$ (for $t \langle 0.01\text{ns}$, $\Delta R \approx t^{\gamma}$, with $\gamma_{55} = 0.95$, $\gamma_{147} = 0.89$, $\gamma_{1289} = 0.95$). For n=55 the late time trajectory has $\Delta R \approx t^{\gamma}$ with a superdiffusive value $\gamma_{55} = 0.65$. This scaling applies not only to the rms ΔR; the entire distribution scales roughly self-similarly. Unlike the power-law distribution, the distributions we find for ΔR at a fixed time separation fall off exponentially. For the 1289-atom cluster and for $t \rangle 0.1\text{ns}$ the cluster sticks in place; $\Delta R(t)$ grows almost not at all, approximately logarithmically, with many oscillations apparent. The n=147 cluster presents an immediate behavior, approximately Brownian, with $\gamma_{55} = 0.43$.

Figure 5-5 shows the distribution of fractional departures from isotropy in the velocity direction as a function of orientation. Several of the tallest spikes in the distribution for n=55 represent extended times when the cluster is not strongly in contact with the surface. Writing $f(\theta) = \Delta N / N$ as a series in $\sin m\theta$ and $\cos m\theta$, we find no statistically significant anisotropy for n=55 or n=147, but for n=1289 there is a significant (5.75-σ) m=2 mode, with amplitude 0.043 peaked along the axis $\theta = 98.5^{o}$ and $\theta = -81.5^{o}$. This is approximately the direction in which the trajectory is extended in Figure 5-2. The curve in the figure includes this m=2 mode plus a marginally significant m=4 mode that makes the contrast between highest and lowest probabilities about 8.8%.

Conclusions

Based on these quantitative statistics and on visualizations of the evolution, we have developed on the following picture. All clusters display a nearly ballistic motion for time intervals

shorter than a few hundred picoseconds. For longer times, longer than about one nanosecond, the lightest cluster continues to move freely over the alkanethiol layer, sliding or rolling over the ends of alkanethiol strands in a motion resembling the activity known as crowd surfing at a concert or sporting event, but with a slightly impeded motion as the alkanethiol strands tug at the surface of the cluster. The motion of the heaviest cluster is much more substantially impeded, resembling that of a tethered balloon buffeted by guts of wind. The frequency spectra reflect this, with a featureless, directionally isotropic spectrum for n=55 cluster, but with pronounced peaks at characteristic scales, different for the *x*- and *y*- components of the motion, for the n=1289 cluster. The behavior of the n=147 cluster lies in between all of these considerations. From the smallest to the largest cluster, the low-frequency power components decrease substantially from one to the next.

In conclusion, we have developed a theoretical understanding of nano-size particle motion on organic assemblies based on large-scale simulations that include a huge numbers of freedom. Unlike motions on solid surfaces, nano-silver particles on organic surfaces can display size-dependent, non-Brownian motions. Our analysis of the transition from super-diffusive motion to localized vibration can apply to a wide range of particle motion on organic surfaces with different sizes.

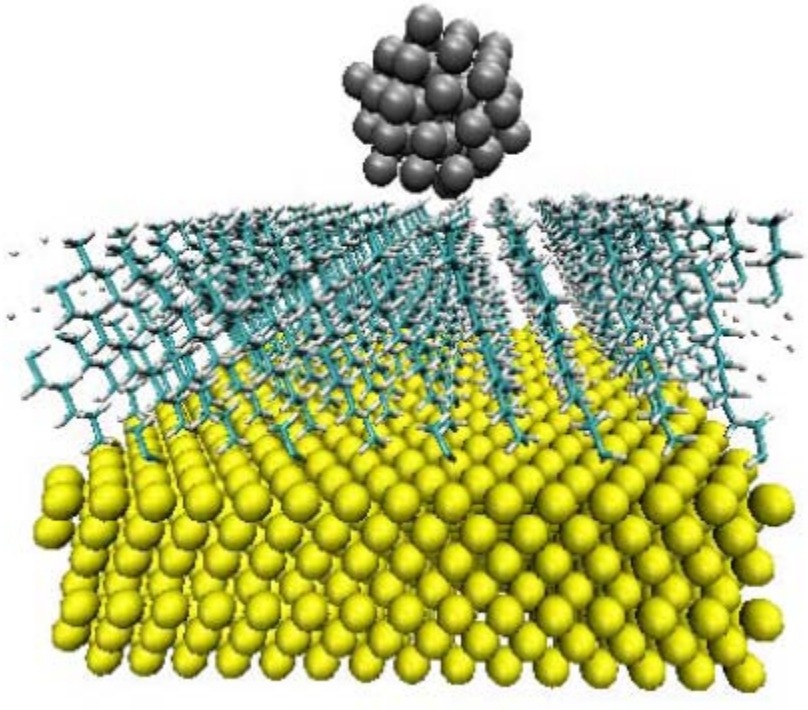

Figure 5-1. Typical cluster/alkanethiol SAM/gold surface configuration for the n=55 cluster. The x- direction is oriented left-right in the picture, the y-direction is out of the page, and z-direction is vertical.

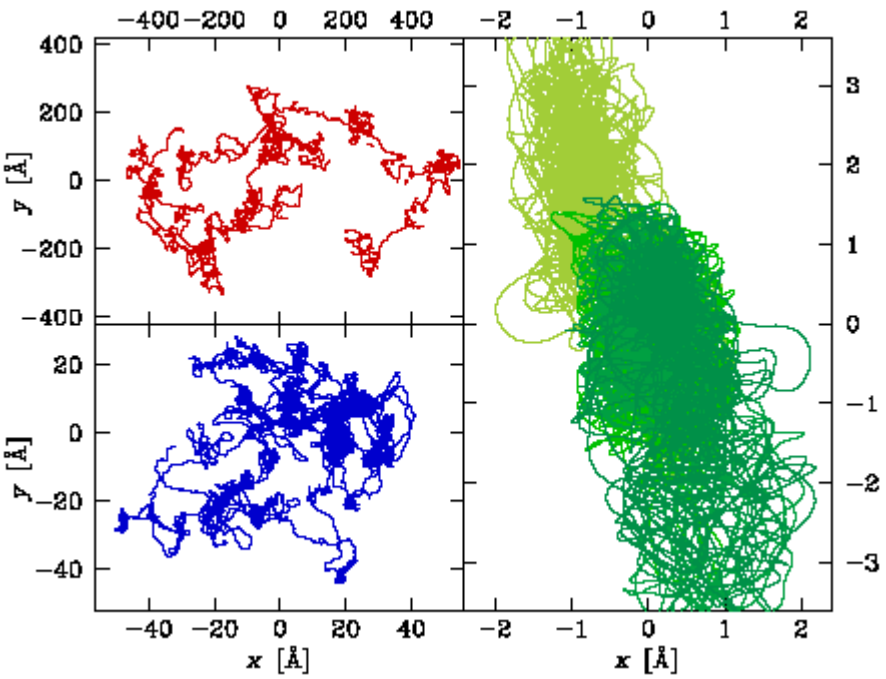

Figure 5-2. Projected x-y trajectories of cluster center of mass for Ag clusters with n=55,147 and 1289 atoms (counterclockwise from top left). For n=1289, darker colors are later in time.

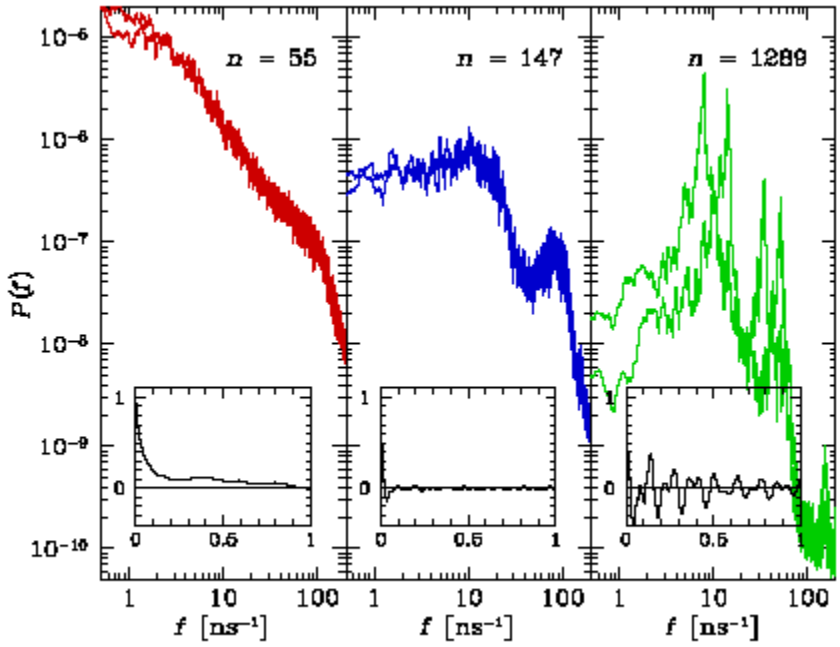

Figure 5-3. Velocity frequency spectra P(f), normalized by velocity variance, as a function of frequency f. Each panel shows the spectrum for both x- and y- components, which are indistinguishable except for n=1289. Spectra are smoothed over a moving window of ±20 points; remaining statistical uncertainties are reflected in the center of the curves. Inserts show the (vector) velocity correlation as a function of time separation t over times from 0 to 1ns.

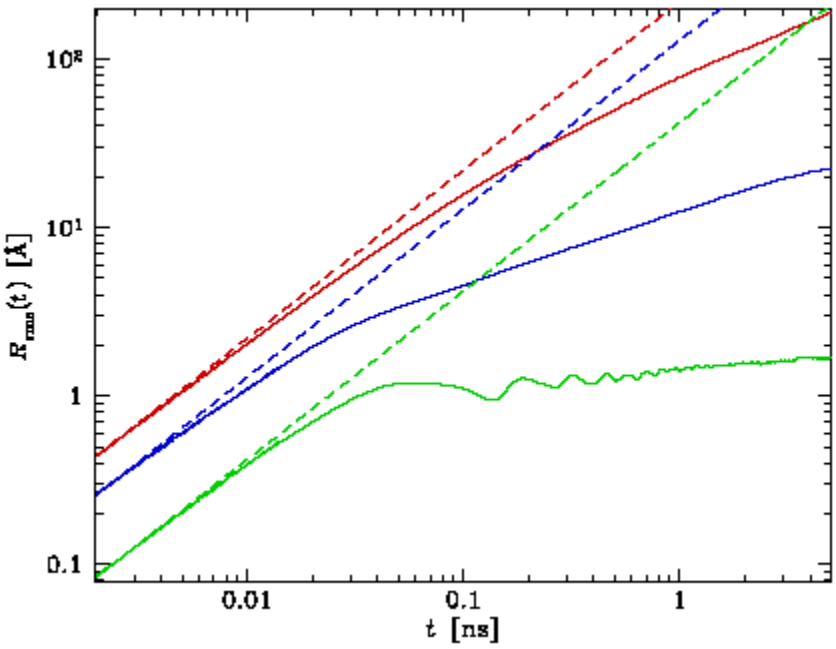

Figure 5-4. Root mean square displacement $\left\langle \Delta R^2(t) \right\rangle^{1/2}$ averaged over a trajectory as a function of time t for n=55, n=147 and n=1289 (top to bottom). Dashed lines show the ballistic limit $\Delta R = \upsilon t$ for thermal velocity $\left\langle \Delta \upsilon^2 \right\rangle = kT/m$; for small times the motion is nearly ballistic.

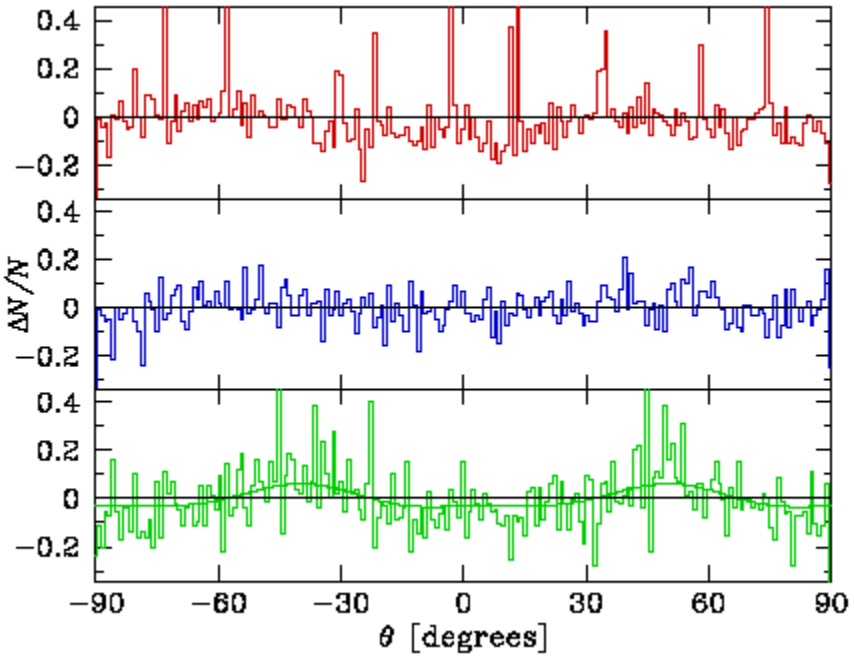

Figure 5-5. Velocity anisotropy: histogram of fractional deviation from isotropy for velocity as a function of direction for n=55, n=147 and n=1289 (top to bottom). Deviations are small, and with similar numbers of points all bins have similar uncertainities, reflected in bin-to-bin scatter.

CHAPTER 6
CONCLUSIONS

In the first project, using classical molecular dynamics, we investigated a homogeneous alkanethiol monolayer and two heterogeneous systems consisting of an alkanethiol monolayer with *cis*- and *trans*- azobenzene molecules on the Au(111) surface. We found that, at a temperature of 350K, all three systems undergo a phase transition from an ordered tilted structure to a vertical, liquid-like structure. A through analysis of temperature dependent properties such as energy, heat capacity, molecular orientation, radial distribution functions, diffusion and local disorder was presented. The results indicate that the phase transition is first-order for these 2-D systems. The global properties of the system, such as the nature of the phase transition, diffusion constants, radial distributions and the transition temperature are not strongly affected by the guest molecules.

In the second project, penetration of Au ad-atoms through alkanethiol SAMS were analyzed. Classical potential parameters were calibrated by quantum-mechanical calculations. We found that Au ad-atoms penetrate the alkanethiol monolayers and form buried layers on the Au/S interface. Our results were in agreement with experiments. At 300K, we observed extensive penetration of Au atoms through the monolayers. At 50K, there was no penetration of Au atoms into the monolayer. As the coverage was increased, formation of layers on the Au/S interface was observed. To achieve agreement with experiments, we scaled the (UFF) parameters by a factor of ten. We also performed DOS and PDOS calculations to analyze the charge transfer between the alkanethiol monolayer and the Au(111) surface.

In the third project, we found that, when Ag clusters are placed on top of alkanethiol monolayers, all clusters show ballistic motion for time intervals shorter than a few hundred picoseconds. If the time interval is longer than 1 ns, the lightest cluster continues to move freely over the alkanethiol layer, sliding and rolling over the surface. This motion is similar to crowd

surfing in a concert or sports event. For the largest cluster, the motion was impeded and it resembled the motion of a tethered balloon. The behavior of the cluster that consists of 147 atoms was intermediate between the two limits. These results were confirmed by frequency spectra. As we move from the smallest to the largest cluster, the low-frequency power component decreases substantially from one to the next.

LIST OF REFERENCES

1. Nuzzo, R. G.; Allara, D. L. *Journal of the American Chemical Society* **1983,** *105,* 4481.

2. Ulman, A. *Chemical Reviews* **1996,** *96,* 1533.

3. Ulman, A.; Evans, S. D.; Shnidman, Y.; Sharma, R.; Eilers, J. E.; Chang, J. C. *Journal of the American Chemical Society* **1991,** *113,* 1499.

4. Kumar, A.; Biebuyck, H. A.; Whitesides, G. M. *Langmuir* **1994,** *10,* 1498.

5. Schreiber, F. *Prog. Surf. Sci.* **2000,** *65,* 151.

6. Dubois, L. H.; Nuzzo, R. G. *Annual Review of Physical Chemistry* **1992,** *43,* 437.

7. Whitesides, G. M.; Ferguson, G. S. *Chemtracts-Org. Chem.* **1988,** *1,* 171.

8. Sellers, H.; Ulman, A.; Shnidman, Y.; Eilers, J. E. *Journal of the American Chemical Society* **1993,** *115,* 9389.

9. Troughton, E. B.; Bain, C. D.; Whitesides, G. M.; Nuzzo, R. G.; Allara, D. L.; Porter, M. D. *Langmuir* **1988,** *4,* 365.

10. Katz, E.; Itzhak, N.; Willner, I. *Journal of Electroanalytical Chemistry* **1992,** *336,* 357.

11. Sabatani, E.; Cohenboulakia, J.; Bruening, M.; Rubinstein, I. *Langmuir* **1993,** *9,* 2974.

12. Bryant, M. A.; Joa, S. L.; Pemberton, J. E. *Langmuir* **1992,** *8,* 753.

13. Hill, W.; Wehling, B. *Journal of Physical Chemistry* **1993,** *97,* 9451.

14. Bain, C. D.; Troughton, E. B.; Tao, Y. T.; Evall, J.; Whitesides, G. M.; Nuzzo, R. G. *Journal of the American Chemical Society* **1989,** *111,* 321.

15. Buck, M.; Eisert, F.; Fischer, J.; Grunze, M.; Trager, F. *Appl. Phys.* **1991,** *53,* 552.

16. Buck, M.; Eisert, F.; Grunze, M.; Trager, F. *Berichte Der Bunsen-Gesellschaft-Physical Chemistry Chemical Physics* **1993,** *97,* 399.

17. Hahner, G.; Woll, C.; Buck, M.; Grunze, M. *Langmuir* **1993,** *9,* 1955.

18. Chidsey, C. E. D.; Liu, G. Y.; Rowntree, P.; Scoles, G. *Journal of Chemical Physics* **1989,** *91,* 4421.

19. Alves, C. A.; Smith, E. L.; Porter, M. D. *Journal of the American Chemical Society* **1992,** *114,* 1222.

20. Scherer, J.; Vogt, M. R.; Magnussen, O. M.; Behm, R. J. *Langmuir* **1997,** *13,* 7045.

21. Jennings, G. K.; Laibinis, P. E. *Colloids and Surfaces a-Physicochemical and Engineering Aspects* **1996,** *116,* 105.

22. Ishibashi, M.; Itoh, M.; Nishihara, H.; Aramaki, K. *Electrochimica Acta* **1996,** *41,* 241.

23. Zamborini, F. P.; Crooks, R. M. *Langmuir* **1998,** *14,* 3279.

24. Feng, Y. Q.; Teo, W. K.; Siow, K. S.; Gao, Z. Q.; Tan, K. L.; Hsieh, A. K. *Journal of the Electrochemical Society* **1997,** *144,* 55.

25. Stratmann, M. *Adv. Mater.* **1990,** *2,* 191.

26. Stratmann, M. *Stahl Und Eisen* **1993,** *113,* 101.

27. Xiao, X. D.; Hu, J.; Charych, D. H.; Salmeron, M. *Langmuir* **1996,** *12,* 235.

28. Kim, H. I.; Graupe, M.; Oloba, O.; Koini, T.; Imaduddin, S.; Lee, T. R.; Perry, S. S. *Langmuir* **1999,** *1,* 3179.

29. Jordan, R.; Ulman, A. *Journal of the American Chemical Society* **1998,** *120,* 243.

30. Luzinov, I.; Julthongpiput, D.; Liebmann-Vinson, A.; Cregger, T.; Foster, M. D.; Tsukruk, V. V. *Langmuir* **2000,** *16,* 504.

31. Sigal, G. B.; Bamdad, C.; Barberis, A.; Strominger, J.; Whitesides, G. M. *Analytical Chemistry* **1996,** *68,* 490.

32. Harrison, D. J.; Mallouk, T. E. *Interfacial Design and Chemical Sensing* **1994,** *561,* 1.

33. Schierbaum, K. D.; Weiss, T.; Vanvelzen, E. U. T.; Engbersen, J. F. J.; Reinhoudt, D. N.; Gopel, W. *Science* **1994,** *265,* 1413.

34. Duan, C. M.; Meyerhoff, M. E. *Analytical Chemistry* **1994,** *66,* 1369.

35. Boulas, C.; Davidovits, J. V.; Rondelez, F.; Vuillaume, D. *Physical Review Letters* **1996,** *76,* 4797.

36. Fujihara, M.; Inokuchi, H. *Chemical Physics Letters* **1972,** *17,* 554.

37. Yang, H. H.; McCreery, R. L. *Analytical Chemistry* **1999,** *71,* 4081.

38. Hautman, J.; Klein, M. L. *Journal of Chemical Physics* **1989,** *91,* 4994.

39. Hautman, J.; Klein, M. L. *Journal of Chemical Physics* **1990,** *93,* 7483.

40. Mar, W.; Klein, M. L. *Langmuir* **1994,** *10,* 188.

41. Bhatia, R.; Garrison, B. J. *Langmuir* **1997,** *13,* 765.

42. Bhatia, R.; Garrison, B. J. *Langmuir* **1997,** *13,* 4038.

43. Beardmore, K. M.; Kress, J. D.; Gronbech-Jensen, N.; Bishop, A. R. *Chemical Physics Letters* **1998,** *286,* 40.

44. Rappe, A. K.; Casewit, C. J.; Colwell, K. S.; Goddard, W. A.; Skiff, W. M. *Journal of the American Chemical Society* **1992,** *114,* 10024.

45. Alkis, S.; Jiang, P.; Wang, L. L.; Roitberg, A. E.; Cheng, H. P.; Krause, J. L. *Journal of Physical Chemistry C* **2007,** *111,* 14743.

46. Leng, Y. S.; Keffer, D. J.; Cummings, P. T. *Journal of Physical Chemistry B* **2003,** *107,* 11940.

47. Sutton, A. P.; Chen, J. *Philosophical Magazine Letters* **1990,** *61,* 139.

48. Yang, Z.; Yang, X. N.; Xu, Z. J. *Journal of Physical Chemistry C* **2008,** *112,* 4937.

49. Yukna, J.; Wang, L. C. *Journal of Physical Chemistry C* **2007,** *111,* 13337.

50. Alamanova, D.; Grigoryan, V. G.; Springborg, M. *Journal of Physical Chemistry C* **2007,** *111,* 12577.

51. Berendsen, H. J. C.; Postma, J. P. M.; Vangunsteren, W. F.; Dinola, A.; Haak, J. R. *Journal of Chemical Physics* **1984,** *81,* 3684.

52. *Molecular Modelling;* Leach, A. R., Eds.; Pearson Education Limited: 1996.

53. Verlet, L. *Physical Review* **1967,** *159,* 98.

54. *The Feynman lectures on physics*; Feynman, R. P.; Leighton, R. B.; Sands, M. L., Eds.; Addison-Wesley Pub. Co.: Reading, 1963.

55. Hohenberg, P.; Kohn, W. *Physical Review B* **1964,** *136,* B864.

56. Vignale, G.; Rasolt, M. *Physical Review Letters* **1987,** *59,* 2360.

57. Kohn, W.; Sham, L. J. *Physical Review* **1965,** *140,* 1133.

58. Kresse, G.; Furthmuller, J. *Physical Review B* **1996,** *54,* 11169.

59. Kresse, G.; Furthmuller, J. *Computational Materials Science* **1996,** *6*, 15.

60. Blöchl, P. E. *Physical Review B* **1994,** *50*, 17953.

61. Perdew, J. P.; Chevary, J. A.; Vosko, S. H.; Jackson, K. A.; Pederson, M. R.; Singh, D. J.; Fiolhais, C. *Physical Review B* **1992,** *46*, 6671.

62. Monkhorst, H. J.; Pack, J. D. *Physical Review B* **1976,** *13*, 5188.

63. Methfessel, M.; Paxton, A. T. *Physical Review B* **1989,** *40*, 3616.

64. Aviram, A.; Ratner, M. A. *Chemical Physics Letters* **1974,** *29*, 277.

65. Reed, M. A.; Zhou, C.; Muller, C. J.; Burgin, T. P.; Tour, J. M. *Science* **1997,** *278*, 252.

66. Pati, R.; Karna, S. P. *Physical Review B* **2004,** *69*, 15.

67. Chen, F.; He, J.; Nuckolls, C.; Roberts, T.; Klare, J. E.; Lindsay, S. *Nano Letters* **2005,** *5*, 503.

68. Flood, A. H.; Ramirez, R. J. A.; Deng, W. Q.; Muller, R. P.; Goddard, W. A.; Stoddart, J. F. *Australian Journal of Chemistry* **2004,** *57*, 301.

69. Emberly, E. G.; Kirczenow, G. *Physical Review Letters* **2003,** *91*, 18.

70. Solak, A. O.; Ranganathan, S.; Itoh, T.; McCreery, R. L. *Electrochemical and Solid State Letters* **2002,** *5*, E43.

71. Gutierrez, R.; Fagas, G.; Cuniberti, G.; Grossmann, F.; Schmidt, R.; Richter, K. *Physical Review B* **2002,** *65*, 11.

72. Baer, R.; Neuhauser, D. *Journal of the American Chemical Society* **2002,** *124*, 4200.

73. Ikeda, T.; Tsutsumi, O. *Science* **1995,** *268*, 1873.

74. Hugel, T.; Holland, N. B.; Cattani, A.; Moroder, L.; Seitz, M.; Gaub, H. E. *Science* **2002,** *296*, 1103.

75. Zhang, C.; Du, M. H.; Cheng, H. P.; Zhang, X. G.; Roitberg, A. E.; Krause, J. L. *Physical Review Letters* **2004,** *92*, 15.

76. Yasuda, S.; Nakamura, T.; Matsumoto, M.; Shigekawa, H. *Journal of the American Chemical Society* **2003,** *125*, 16430.

77. Wen, Y. Q.; Yi, W. H.; Meng, L. J.; Feng, M.; Jiang, G. Y.; Yuan, W. F.; Zhang, Y. Q.; Gao, H. J.; Jiang, L.; Song, Y. L. *Journal of Physical Chemistry B* **2005,** *109*, 14465.

78. Chen, J.; Reed, M. A.; Asplund, C. L.; Cassell, A. M.; Myrick, M. L.; Rawlett, A. M.; Tour, J. M.; Van Patten, P. G. *Applied Physics Letters* **1999,** *75*, 624.

79. Arnold, S.; Feng, Z. Q.; Kakiuchi, T.; Knoll, W.; Niki, K. *Journal of Electroanalytical Chemistry* **1997,** *438*, 91.

80. *Molecular nanoelectronics*; Reed, M. A.; Takhee, L., Eds.; American Scientific Publishers: Steven Ranch, CA, 2003.

81. Yonzon, C. R.; Haynes, C. L.; Zhang, X. Y.; Walsh, J. T.; Van Duyne, R. P. *Analytical Chemistry* **2004,** *76*, 78.

82. Camillone, N.; Chidsey, C. E. D.; Liu, G. Y.; Putvinski, T. M.; Scoles, G. *Journal of Chemical Physics* **1991,** *94*, 8493.

83. Li, Y. Z.; Huang, J. Y.; Mciver, R. T.; Hemminger, J. C. *Journal of the American Chemical Society* **1992,** *114*, 2428.

84. Dubois, L. H.; Zegarski, B. R.; Nuzzo, R. G. *Journal of Chemical Physics* **1993,** *98*, 678.

85. Camillone, N.; Eisenberger, P.; Leung, T. Y. B.; Schwartz, P.; Scoles, G.; Poirier, G. E.; Tarlov, M. J. *Journal of Chemical Physics* **1994,** *101*, 11031.

86. Clark, S. L.; Montague, M.; Hammond, P. T. *Supramolecular Science* **1997,** *4*, 141.

87. Kondoh, H.; Kodama, C.; Sumida, H.; Nozoye, H. *Journal of Chemical Physics* **1999,** *111*, 1175.

88. Terrill, R. H.; Postlethwaite, T. A.; Chen, C. H.; Poon, C. D.; Terzis, A.; Chen, A. D.; Hutchison, J. E.; Clark, M. R.; Wignall, G.; Londono, J. D.; Superfine, R.; Falvo, M.; Johnson, C. S.; Samulski, E. T.; Murray, R. W. *Journal of the American Chemical Society* **1995,** *117*, 12537.

89. Donhauser, Z. J.; Mantooth, B. A.; Kelly, K. F.; Bumm, L. A.; Monnell, J. D.; Stapleton, J. J.; Price, D. W.; Rawlett, A. M.; Allara, D. L.; Tour, J. M.; Weiss, P. S. *Science* **2001,** *292*, 2303.

90. Lewis, P. A.; Inman, C. E.; Yao, Y. X.; Tour, J. M.; Hutchison, J. E.; Weiss, P. S. *Journal of the American Chemical Society* **2004,** *126*, 12214.

91. Tejwani, M. J.; Ferreira, O.; Vilches, O. E. *Physical Review Letters* **1980,** *44*, 152.

92. Poirier, G. E.; Tarlov, M. J. *Langmuir* **1994,** *10*, 2853.

93. Camillone, N.; Chidsey, C. E. D.; Liu, G.; Scoles, G. *Journal of Chemical Physics* **1993,** *98*, 4234.

94. Fenter, P.; Eisenberger, P.; Liang, K. S. *Physical Review Letters* **1993,** *70*, 2447.

95. Barrena, E.; Ocal, C.; Salmeron, M. *Journal of Chemical Physics* **1999,** *111*, 9797.

96. Zhang, Z.; Beck, T. L.; Young, J. T.; Boerio, F. J. *Langmuir* **1996,** *12*, 1227.

97. Zhang, L. Z.; Goddard, W. A.; Jiang, S. Y. *Journal of Chemical Physics* **2002,** *117*, 7342.

98. Fischer, D.; Curioni, A.; Andreoni, W. *Langmuir* **2003,** *19*, 3567.

99. Mayo, S. L.; Olafson, B. D.; Goddard, W. A. *Journal of Physical Chemistry* **1990,** *94*, 8897.

100. Jung, H. H.; Do Won, Y.; Shin, S.; Kim, K. *Langmuir* **1999,** *15*, 1147.

101. Finnis, M. W.; Sinclair, J. E. *Philosophical Magazine a-Physics of Condensed Matter Structure Defects and Mechanical Properties* **1984,** *50*, 45.

102. Schulze, F. W.; Petrick, H. J.; Cammenga, H. K.; Klinge, H. *Zeitschrift Fur Physikalische Chemie-Frankfurt* **1977,** *107*, 1.

103. Perdew, J. P.; Burke, K.; Ernzerhof, M. *Physical Review Letters* **1996,** *77*, 3865.

104. Yourdshahyan, Y.; Zhang, H. K.; Rappe, A. M. *Physical Review B* **2001,** *8*, 6308.

105. Gronbeck, H.; Curioni, A.; Andreoni, W. *Journal of the American Chemical Society* **2000,** *122*, 3839.

106. Mazzarello, R.; Cossaro, A.; Verdini, A.; Rousseau, R.; Casalis, L.; Danisman, M. F.; Floreano, L.; Scandolo, S.; Morgante, A.; Scoles, G. *Physical Review Letters* **2007,** *98*, 1.

107. Camillone, N.; Chidsey, C. E. D.; Eisenberger, P.; Fenter, P.; Li, J.; Liang, K. S.; Liu, G. Y.; Scoles, G. *Journal of Chemical Physics* **1993,** *99*, 744.

108. Fenter, P.; Eberhardt, A.; Liang, K. S.; Eisenberger, P. *Journal of Chemical Physics* **1997,** *106*, 1600.

109. Wink, T.; vanZuilen, S. J.; Bult, A.; vanBennekom, W. P. *Analyst* **1997,** *122*, 43.

110. Gooding, J. J.; Praig, V. G.; Hall, E. A. H. *Analytical Chemistry* **1998,** *70*, 2396.

111. Chen, J.; Reed, M. A.; Rawlett, A. M.; Tour, J. M. *Science* **1999,** *286*, 1550.

112. Zhu, Z. H.; Daniel, T. A.; Maitani, M.; Cabarcos, O. M.; Allara, D. L.; Winograd, N. *Journal of the American Chemical Society* **2006,** *128*, 13710.

113. Stoliar, P.; Kshirsagar, R.; Massi, M.; Annibale, P.; Albonetti, C.; de Leeuw, D. M.; Biscarini, F. *Journal of the American Chemical Society* **2007,** *129*, 6477.

114. Asadi, K.; Gholamrezaie, F.; Smits, E. C. P.; Blom, P. W. M.; de Boer, B. *Journal of Materials Chemistry* **2007,** *17*, 1947.

115. Jung, D. R.; Czanderna, A. W. *Critical Reviews in Solid State and Materials Sciences* **1994,** *19*, 1.

116. Wang, B.; Xiao, X. D.; Sheng, P. *Journal of Vacuum Science & Technology B* **2000,** *18*, 2351.

117. Ohgi, T.; Sheng, H. Y.; Nejoh, H. *Applied Surface Science* **1998,** *132*, 919.

118. Hooper, A.; Fisher, G. L.; Konstadinidis, K.; Jung, D.; Nguyen, H.; Opila, R.; Collins, R. W.; Winograd, N.; Allara, D. L. *Journal of the American Chemical Society* **1999,** *121*, 8052.

119. Tighe, T. B.; Daniel, T. A.; Zhu, Z. H.; Uppili, S.; Winograd, N.; Allara, D. L. *Journal of Physical Chemistry B* **2005,** *109*, 21006.

120. Jiang, S. Y. *Molecular Physics* **2002,** *100*, 2261.

121. Hietpas, G. D.; Sands, J. M.; Allara, D. L. *Macromolecules* **1998,** *31*, 3374.

122. Xiong, Z. H.; Wu, D.; Vardeny, Z. V.; Shi, J. *Nature* **2004,** *427*, 821.

123. Akkerman, H. B.; Blom, P. W. M.; de Leeuw, D. M.; de Boer, B. *Nature* **2006,** *441*, 69.

124. Selzer, Y.; Cai, L. T.; Cabassi, M. A.; Yao, Y. X.; Tour, J. M.; Mayer, T. S.; Allara, D. L. *Nano Letters* **2005,** *5*, 61.

125. Chaki, N. K.; Vijayamohanan, K. *Biosensors & Bioelectronics* **2002,** *17*, 1.

126. Maxwell, D. J.; Taylor, J. R.; Nie, S. M. *Journal of the American Chemical Society* **2002,** *124*, 9606.

127. *Nanobiotechnology*; Niemeyer, C. M.; Mirkin, C. A., Eds.; Wiley-VCH: Weinheim, 2004.

128. *Nanobiotechnology: more concepts and applications*; Mirkin, C. A.; Niemeyer, C. M., *Eds.;* Wiley-VCH: Weinheim, 2007.

129. *Surface Diffusion: Atomistic and Collective Processes*; Tringides, M. C., Eds.; Plenum Press: New York, 1997.

130. *Collective diffusion on surfaces: Correlation effects and adatom interactions*; Tringides, M. C.; Chvoj, Z., Eds.; Kluwer Academic: Dodrecht, 2001.

131. Luedtke, W. D.; Landman, U. *Physical Review Letters* **1999,** *82*, 3835.

132. *Metal clusters at surfaces: Structure, quantum properties, physical chemistry*; Meiwes-Broer, K. H., Eds.; Springer: Berlin/New York, 2000.

133. Tarlov, M. J. *Langmuir* **1992,** *8*, 80.

134. Hostetler, M. J.; Wingate, J. E.; Zhong, C. J.; Harris, J. E.; Vachet, R. W.; Clark, M. R.; Londono, J. D.; Green, S. J.; Stokes, J. J.; Wignall, G. D.; Glish, G. L.; Porter, M. D.; Evans, N. D.; Murray, R. W. *Langmuir* **1998,** *14*, 17.

135. Mulvaney, P. *Langmuir* **1996,** *12*, 788.

136. Chen, S. H.; Fan, Z. Y.; Carroll, D. L. *Journal of Physical Chemistry B* **2002,** *106*, 10777.

137. Palmer, R. E.; Pratontep, S.; Boyen, H. G. *Nature Materials* **2003,** *2*, 443.

138. Leung, C.; Xirouchaki, C.; Berovic, N.; Palmer, R. E. *Advanced Materials* **2004,** *16*, 223.

139. *Clusters and nano-assemblies: Physical and biological systems*; Jena, P.; Khanna, S. N.; Rao, B. K., Eds.; World Scientific Publications: Singapore/New York, 2005.

140. Cheng, H. P.; Landman, U. *Science* **1993,** *260*, 1304.

141. Cheng, H. P.; Landman, U. *Journal of Physical Chemistry* **1994,** *98*, 3527.

142. Widrig, C. A.; Chung, C.; Porter, M. D. *Journal of Electroanalytical Chemistry* **1991,** *310*, 335.

143. Alloway, D. M.; Hofmann, M.; Smith, D. L.; Gruhn, N. E.; Graham, A. L.; Colorado, R.; Wysocki, V. H.; Lee, T. R.; Lee, P. A.; Armstrong, N. R. *Journal of Physical Chemistry B* **2003,** *107*, 11690.

144. Xu, W.; Szulczewski, G. J.; LeClair, P.; Navarrete, I.; Schad, R.; Miao, G.; Guo, H.; Gupta, A. *Applied Physics Letters* **2007,** *90*, 7.

BIOGRAPHICAL SKETCH

Sabri Alkis was born in Turkey in the year 1981. He went to high school in Bursa Fen Lisesi. He got a B.S. in chemistry from Bilkent University in 2004. He developed alkaline fuel cells under the direction of Dr. Borovsky. In the summer 2003, he attended a summer research programme in Max Planck Institute for Colloids and did research with Dr. Colfen. He started graduate school at the University of Florida and he specialized in computational nanotechnology under the direction of Dr. Krause and Dr. Cheng. He received a Ph.D. in chemistry in the year 2009.